THESIS

EXPERIMENTAL INVESTIGATION OF AUTOMOTIVE REFUELING SYSTEM FLOW AND EMISSIONS DYNAMICS TO SUPPORT CFD DEVELOPMENT

Submitted by

T. McKay Stoker

Department of Mechanical Engineering

In partial fulfillment of the requirements

For the Degree of Master of Science

Colorado State University

Fort Collins, Colorado

Summer 2019

Master's Committee:

Advisor: Bret C. Windom

Shantanu Jathar
Ellison Carter

ABSTRACT

EXPERIMENTAL INVESTIGATION OF AUTOMOTIVE REFUELING SYSTEM FLOW AND EMISSIONS DYNAMICS TO SUPPORT CFD DEVELOPMENT

Government regulations restrict the evaporative emissions during refueling to 0.20 grams per gallon of dispensed fuel. This requires virtually all of the vapors generated and displaced while refueling to be stored onboard the vehicle. The refueling phenomenon of spit-back and early click-off are also important considerations in designing refueling systems. Spit-back is fuel bursting past the nozzle and into the environment and early click-off is the pump shutoff mechanism being triggered before the tank is full. Both are detrimental to customer satisfaction, and spit-back leads to failing government regulations. Development of a new refueling system design is required for each vehicle as packaging requirements change. Each new design (or redesign) must be prototyped and tested to ensure government regulations and customer satisfaction criteria are satisfied. Often designs need multiple iterations, costing money and time in prototype-based validation procedures. To conserve resources, it is desired to create a Computational Fluid Dynamics (CFD) tool to assist in design validation. To aid in creating such a model, controlled experiments were performed to inform and validate simulations. The simulations and experiments were performed on the same in-production refueling system. Test data provided characterization of non-trivial boundary conditions. Refueling experiments gave points of comparison for CFD results, especially the tank pressure. Finally, collection of emissions data during refueling experiments provided insight into the travel of gasoline vapor in

the refueling system. All the information gathered provides greater understanding of the refueling process and will aid the continued development of CFD models for refueling.

ACKNOWLEDGEMENTS

I would like to thank my advisor, Dr. Bret Windom, for his support. Working on this research has allowed me to greatly improve my skills. Dr. Windom has always encouraged me, and gave me all the knowledge and help I needed. His guidance has been much appreciated.

Gratitude goes to my exam committee, Dr. Shantanu Jathar and Dr. Ellison Carter. Their participation and review of my thesis was crucial.

Honda R&D Americas, Inc. deserves special thanks for their support of this project. From financial support, equipment generosity, and engineer expertise, this work would not have been possible without them. Marc Henderson was particularly valuable for his direction, guidance, coordination, and help in weekly meetings and at other times. Joshua Shaw also contributed greatly with his knowledge of refueling systems and thoughtful reviews that improved this thesis and other project dissemination opportunities.

Mangesh Dake was the brilliant graduate student behind the CFD side of the project. As he started on the project a year prior to my arrival, he was my direct teacher. I am very grateful for his initial and ongoing help. I am also appreciative to the senior design team that helped with Phase I of this work. They did much in the experimental setup used throughout the study. Luke Nibbelink was especially dedicated and also assisted in creating figures used in a technical paper and in this thesis.

My appreciation and thanks go especially to my wife, Chaia. She has given me the most support and encouragement. She always believed in me, even on very hard days. She also coordinated to allow me to work late and served as my assistant for many experiments to be presented here. I could not have completed this research without her.

TABLE OF CONTENTS

1. Introduction

The evaporative emissions from the automobile refueling process are regulated by the Environmental Protection Agency (EPA). This is due to the polluting nature of the hydrocarbon (HC) vapors. HC vapors are Volatile Organic Compounds (VOCs), which contribute to ground-level ozone and smog [1, 2]. An automobile fuel tank contains HC vapors mixed with air in a space above the liquid fuel level, known as the headspace. During refueling, the headspace mixture must be displaced as liquid fuel fills the tank. Historically, many of the displaced HC vapors have been released into the atmosphere, causing much pollution. Thus, the EPA has regulated the emissions produced from the refueling process [3].

Refueling emissions regulations also reduce individual exposure to HC vapors. Exposure to benzene, a HC compound found in gasoline, has been linked to increased risk of cancer [4, 5]. Automobile refueling is the major source of benzene exposure for non-smoking individuals [6, 7]. Thus, regulating refueling emissions reduces human exposure to this harmful substance.

Initially, the EPA mandated that gasoline stations control refueling HC emissions. This was done using "Stage II" vapor recovery systems. Stage II systems consisted of a boot that surrounded the pump nozzle, meant to fit tightly around the opening of the vehicle's filler pipe, where the nozzle is inserted. Inside the boot was a suction device that pulled vapors escaping the filler pipe into the station's underground storage tank. Then they could condense back into the liquid fuel [8].

Stage II vapor recovery systems proved difficult to implement, manage, and regulate. Their performance was also poor and the systems would steadily degrade [8]. Therefore, the EPA deregulated Stage II recovery systems and placed the burden of controlling refueling

emissions on automotive Original Equipment Manufacturers (OEMs) [9, 10]. This led to widespread use of Onboard Refueling Vapor Recovery (ORVR) systems. ORVR systems keep virtually all of the displaced vapors on the vehicle, either by condensation back into the liquid or by adsorption in the activated-carbon canister. Vapors in the canister are purged later, when they are drawn into the engine for combustion under certain driving conditions.

The impact of evaporative and refueling emissions control (EVAP/ORVR) can be seen through a simple illustration. An estimation for emissions and gasoline loss without EVAP/ORVR was presented in a Society of Automotive Engineers (SAE) training on the subject. Emissions are estimated to be 6 billion grams per day, which equates to 2.13 million gallons of gasoline lost per day. This would be 0.5% of the 390 million gallons of gasoline consumed in the United States (US) each day [11]. From a mathematical model developed by Reddy, refueling HC generation is calculated to be 4.10 grams for each gallon dispensed (g/gal) under the EPA test conditions [12]. Though refueling conditions vary widely, the EPA conditions offer a point for comparison. Without ORVR, refueling operations for the daily US gasoline consumption would cause 1.6 billion grams of HC emissions, 567 thousand gallons of gasoline lost. This accounts for 27% of the total uncontrolled evaporative losses. With ORVR systems achieving the EPA regulation of 0.20 g/gal [3], emissions are reduced to 78 million grams and gasoline losses are reduced to 27.6 thousand gallons per day, a reduction of 95%.

Figure 1 depicts the refueling system and process. As liquid fuel displaces the headspace gases, there are two paths for the air/vapor mixture to take. One path is through the activated-carbon canister, where HC vapors are adsorbed and clean air passes through. The other path is through the Vapor Return Line (VRL) and back into the fuel filler pipe. This second path reduces pressure in the tank, allows some vapors to be entrained back into the liquid fuel, and reduces

fresh air entrainment and subsequent increased evaporation. Once the liquid fuel closes both vapor exits, tank pressure builds rapidly. The increased pressure causes a liquid column to build in the fuel filler pipe until the fuel reaches the nozzle. An air entrainment port on the nozzle serves as the automatic shutoff mechanism. During refueling, the port entrains air into the dispensed fuel by a Venturi effect. When covered by liquid fuel, a vacuum is created, causing a valve to close and stop fuel flow.

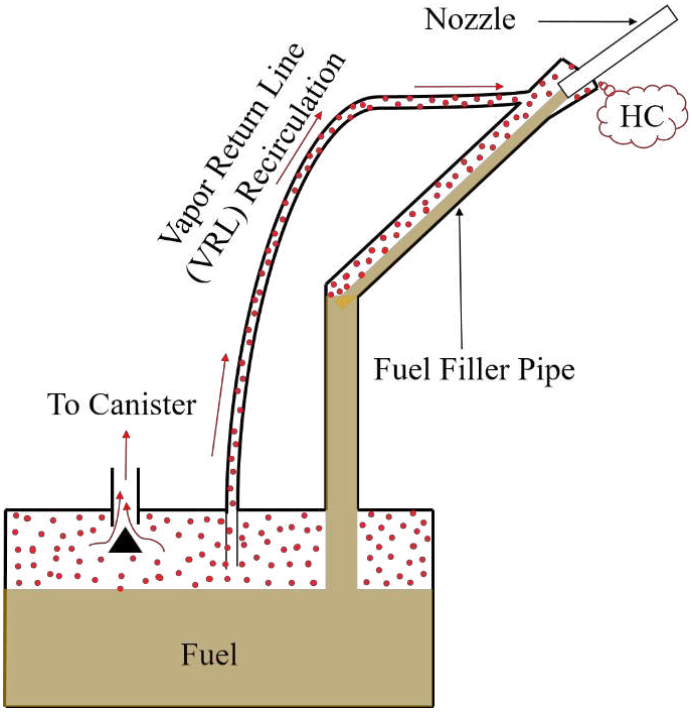

Figure 1: Schematic of the refueling process.

In proper operation, with a sealed system and appropriately sized canister, any HC vapors leaving the system would escape via the fuel filler pipe. With the nozzle inserted, the filler pipe is not completely sealed from the environment and vapors may escape into the atmosphere. The current EPA regulation allows for a maximum of 0.20 grams of HC vapor to escape into the atmosphere for each gallon of fuel dispensed (g/gal) during a standardized test [3]. To achieve this, without needing an overly large and expensive canister, an appropriate split of vapor flow

between the canister and the VRL must be achieved. The refueling system must also be free of spit-back, where liquid fuel exits past the nozzle and into the environment.

For customer satisfaction, the phenomenon of early click-off, when the pump nozzle shuts off before the tank is full, should also be avoided. This may also be referred to as Premature Shutoff (PSO). Normal Shutoff (NSO) is used to describe filling of the tank to capacity before the pump automatic shutoff is triggered. The phenomenon of spit-back is also undesirable for customer satisfaction.

To ensure a refueling system design meets customer requirements and EPA regulations, it is prototyped and tested. Often, a design will not meet all requirements or a design change is necessary for other reasons, such as changing packaging requirements. This triggers another round of designing, prototyping, and testing. These validation procedures are costly to OEMs, both in terms of time and money.

Due to the high cost of validating the performance of a refueling system, a Computational Fluid Dynamics (CFD) model capable of accurate simulation of the process is desired. Such a model would provide design guidance and detection of poor designs before any prototypes are made, thus saving OEM resources. Ideally, the CFD model would run quickly enough to also provide time savings over traditional validation procedures.

For CFD simulations to be accurate, however, they need experimental data to inform and validate their predictions. Boundary conditions are critical to any CFD accuracy. Characterizing boundaries with test data allows correct modeling in simulations. Such tests are also important to justify assumptions that can be critical in simplifying calculations and shortening run time, ultimately enhancing the usefulness of the simulation. Other experiments done to allow

comparison with CFD results validate the accuracy of model predictions. The experimental work presented in the following chapters has supported the development of a refueling CFD model.

1.1 Thesis Organization

The current work involved experiments performed to understand dynamics of the refueling system and process. Though a CFD model will be discussed and simulation results shown, note that the CFD work was done by another graduate student. Discussion of the CFD model is only to provide context for the current work. The study has been divided into two parts, named Phase I and Phase II. Phase I investigated the flow dynamics of a system with negligible evaporation. Results of this phase were used to inform and validate CFD simulations without evaporation/condensation modeling. Phase II investigated the emissions dynamics from the refueling system and the effect of varying backpressures of the vapor paths.

Chapter 2 will give background on relevant topics. The EPA refueling test procedure and description of the refueling system will be discussed. A literature review of previous experimental and computational studies will be presented. Finally, a general background of important CFD modeling will be given.

Chapter 3 presents details of the setup of the two phases. Here, the differences in the experiments of the two phases will be shown. Equipment used for fuel delivery and data acquisition will be described. Procedure of the two phases will be outlined.

Chapter 4 presents results and discussion for the two phases. Phase I results provide validation to the initial full system CFD model. Phase II results show trends in the emissions dynamics and timing. The effects of different vapor path backpressures is also observed.

Finally, Chapter 5 briefly summarizes the conclusions of the study. Conclusions are made regarding the capability of refueling CFD simulations and phenomena discovered by the experiments. Future work is recommended to further the findings presented here.

2. Background

2.1 ORVR System Background

The activated-carbon canister is the main component of the ORVR system. As the headspace mixture passes through the canister, the activated-carbon adsorbs HCs while letting air pass through into the environment. The canister's connection to the atmosphere also allows the tank to have zero gauge pressure when not refueling. Then, under part-throttle driving, a manifold vacuum is created and air is pulled through the canister, desorbing the HC vapor and carrying it to the engine for combustion. This process, called purging, allows the canister to continue to be used. The activated carbon can sustain the large number of adsorption and desorption cycles throughout the life of the vehicle without deteriorating [11].

Many ORVR systems also include a recirculation line, here referred to as the Vapor Return Line (VRL). The VRL connects the headspace of the tank to some point in the fuel filler pipe, often near the entrance. This provides a second path for headspace gases to escape. Ideally, as the headspace mixture is introduced to the filler pipe, the liquid fuel rushing past creates a Venturi effect, pulling the gases down the filler pipe. The goal of the recirculation is to entrain and condense some of the HC vapors back into the liquid fuel. Additionally, the fresh air entrainment from the environment will be reduced, consequently reducing new vapor generation.

Introducing vapors into the fuel filler pipe through the VRL creates the possibility for them to escape into the atmosphere, either by reversed gas flow or diffusion. As more vapors are introduced through the VRL, the fuel flow may not be able to entrain them all. This problem may be avoided by removing the VRL and increasing the canister capacity. However, canister size minimization is favorable to OEMs because of the cost of activated carbon. Thus, the flow

between the two vapor paths, the activated-carbon canister and the VRL, is tuned to achieve the EPA standards while reducing canister size.

2.2 EPA Test Description

The standardized EPA test measures the mass of HC vapor emitted during refueling using a Sealed Housing for Evaporative Determination (SHED). SHEDs are completely sealed units. A SHED may have volume compensation to allow a constant pressure in the chamber as temperature changes. This is useful for EPA diurnal evaporative emissions tests but unnecessary for refueling tests, which are performed at a constant temperature. For evaporative emissions tests, Variable Temperature SHEDs (VT-SHEDs) are typically used. VT-SHEDs have temperature control and are an easy way to soak the tank and pre-filled fuel at the specified temperature for the refueling test. A sampling system sends the gas mixture inside the SHED to a Flame Ionization Detector (FID), which measures the HC concentration of the sample. A special gasoline formulation called indolene is specified for the test. It has no ethanol content. The tank is filled with 10% of its capacity; this is referred to as the pre-fill. The tank and pre-fill are allowed to soak at 80^{o}F for at least 6 hours and up to a maximum of 24 hours prior to the test. Just prior to the test, the "dummy" canister is removed and replaced with the conditioned test canister. The nozzle is inserted into the fuel filler pipe or the fuel filler cap is removed and the SHED door is sealed within two minutes. The FID trace is allowed to stabilize. Within 10 minutes of sealing the door, an initial HC concentration is recorded. The HC concentration at this time is set as the zero point. During the test, the incoming fuel is kept at 67 ± 1.5^{o}F. The indolene used must have a Reid Vapor Pressure (RVP) of 9 psi. RVP is the vapor pressure of a liquid at 100^{o}F using the ASTM D-323 standard. The flow rate is 9.8 ± 0.3 gallons per minute (GPM). The tank is filled to at least 95% of its nominal capacity and then the nozzle is left in the filler

pipe for an additional minute. Data is recorded during the fill and for the minute after click-off. The HC concentration measurement is recorded at this point. With a knowledge of the volume of the SHED and the density of the vapors, the total mass of HCs emitted is calculated. This is then divided by the volume of fuel dispensed to get the final g/gal result. The test may be repeated, at fuel flow rates between 4.0 and 9.8 GPM [3].

2.3 Literature Review

There are many previous studies regarding the refueling process in automobiles. Articles, academic theses, and other sources are reviewed in this section. As the present experimental work has and will be used to enable Computer Aided Engineering (CAE) of refueling systems, both experimental and computational literature will be discussed.

Previous refueling CAE works have only modeled components of the refueling system, or modeled the entire system using overly-simplified physics or components. Banerjee et al. (2001) performed CFD analysis of a refueling system, using commercial CFD software FLUENT 5.0 [13]. They used the Volume of Fluid (VOF) method to allow simulation of air and gasoline together. Their results showed good agreement with previous experimental work, and highlighted design elements and processes of importance. However, their tank was a simple rectangle and the nozzle was simulated as a straight tube. They also excluded the complex VRL boundary.

In a 2002 technical paper, Banerjee et al. presented results of simulations of critical components in the ORVR system [14]. They investigated the filler pipe, tank, canister, recirculation tube (another term for the VRL), and the gasoline pump nozzle. Insights from this study include pressure variations at critical locations in the refueling system (bottom of the filler pipe, tank headspace, and the canister inlet and outlet). They also concluded that a surrogate for

gasoline, in this case water, cannot capture all the flow phenomena of the actual fluid. The CFD simulations were informed and validated with comparable experiments. Evaporation was also included in this model and vapor generation was estimated. Air entrainment in the nozzle was measured, but the simulations were done without this data. The simulated nozzle inlet was completely comprised of liquid. The filler pipe outlet was assumed to be at atmospheric conditions, neglecting the tank and its pressure profile.

The work of aus der Wiesche (2004) focused only on the filler pipe flow [15]. They used VOF modeling to track the interface between air and liquid fuel. Evaporation modeling was not considered in this study. The filler pipe simulated was an in-production design. Though not rigorously validated with directly comparable experiments, the model provided insight into trends and the capabilities of CFD. The author also optimized the shape of the filler pipe outlet to reduce its pressure drop, and this decrease was confirmed by test data.

A thesis by Gunnesby (2015) simulated both a simplified filler pipe design and a production unit [16]. No attempt to model evaporation was made. Instead, the flow patterns in the filler pipe were investigated with water and diesel, which both have negligible evaporation. First, a simple filler pipe was constructed and hooked into an open tank. Water was used in this stage. Next, a production filler pipe connected to a production tank was studied. Diesel fuel flowing at 55 liters/minute (LPM) was used. The simulation incorporated a tank, but neglected several internal components. With a clear filler pipe, visuals were obtained from experiment. They matched qualitatively to images from the CFD. Fair agreement was obtained between filler pipe and tank pressures. However, the simulation was only made to calculate the first second of refueling. This was done to capture many of the transient flow considerations and save computational time. Gunnesby simplified the nozzle to a straight tube, in both CFD and

experiment, for the simplified case. The production component case used a true nozzle in testing, but the simulations only contained a simple inlet. Inaccurate modeling of the nozzle spray was cited as a probable cause of discrepancies. Thus, the inlet condition is vital to accurate simulations.

Dake et al. (2018) performed experiments and simulations to determine how best to model the refueling nozzle [17]. They measured the amount of air entrained in the nozzle during operation at multiple flow rates. This volume fraction of air was applied to the nozzle's inlet flow boundary. Several designs were tried to determine the necessary complexity of the model to capture the experimental spray pattern. This was determined as the width of the spray 250 mm from the nozzle tip. Designs ranged from a circle to the entire nozzle geometry. Two different production nozzles were studied: a Husky X1 and an OPW 11B. Figure 2 depicts the geometry of the nozzles. The authors determined that the nozzle geometry up to the check valve should be modeled. Figure 3 shows a comparison of experiment and simulation results for the OPW nozzle when the nozzle is modeled in this manner. The actual air entrainment mechanism may be modeled also, but this adds little accuracy at much greater computational expense. Instead, the volume fraction of air may be specified at the inlet boundary. Their work showed that simulation can accurately capture the characteristics of the nozzle. They also show the importance of the nozzle boundary condition for refueling simulations. Their recommendations were used in all simulation results presented here.

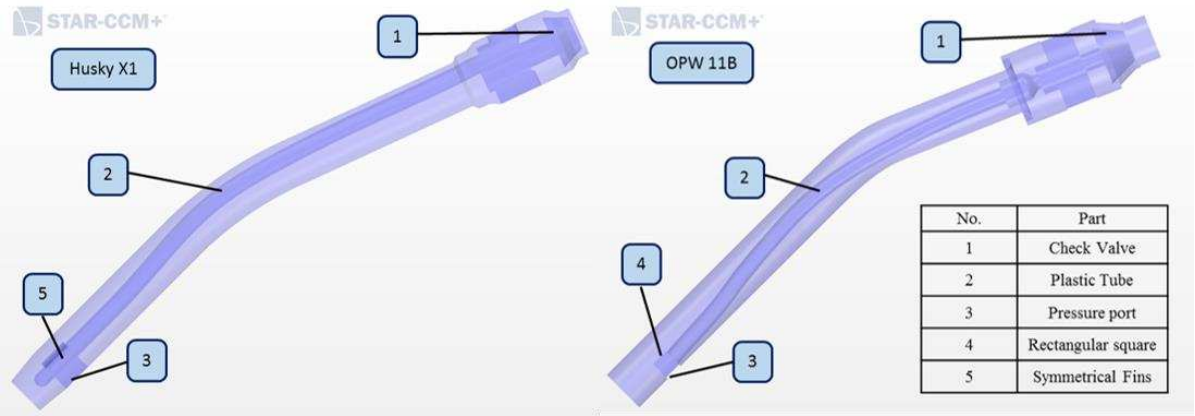

Figure 2: Diagrams for internal geometries of Husky X1 and OPW 11B nozzles. Note location 1, the Check Valve.

Figure 3: Comparison of experimental and simulated spray widths from Dake et al. for the OPW 11B nozzle at 4 and 6 GPM.

Cingle and McClement published a study on uncontrolled (no ORVR) automotive refueling emissions in 1988 [18]. They studied emissions from refueling of 22 late-model vehicles. The goal of their study was to identify the effects of fuel RVP, dispensed fuel temperature, differential temperature (between the tank and the dispensed fuel), and tank and fuel filler pipe geometry on refueling emissions. Fuel RVP, dispensed fuel temperature, and differential temperature were significant factors. Though a variety of tank and filler pipe geometries were tested, these geometries did not significantly affect refueling emissions.

Yamada et al. studied refueling emissions from eight Japanese market cars in 2015 [19]. At the time of publication, Japan had no refueling emission regulation. Thus, the cars were not

equipped with ORVR systems. They found the refueling emissions from the test vehicles at 20ºC to be 1.02 ± 0.40 g/L (3.86 ± 1.5 g/gal), well above the 0.20 g/gal EPA limit. They also investigated the composition of refueling emissions using Proton Transfer Reaction plus Switchable Reagent Ion mass spectrometry (PTR + SRI-MS). By mass, the emissions consist of 80% alkanes and 20% alkenes. Aromatics and di-enes are negligible. Japanese real-world fuel was used.

Mastroianni (2000) conducted an experimental investigation of automobile refueling in their thesis [20]. The tank was not a production unit but a clear, rectangular unit created specifically for the study. Tests were conducted with varying fuel flow rates, vent tube (VRL) inside diameters, and RVP values of the fuel. It was discovered that the smallest vent tube inside diameter (3.2 mm) caused early click-off in each case. Increases in fuel RVP and fuel flow rate were found to increase tank dome pressure, or pressure in the headspace. Between the two factors, fuel RVP was more effective in increasing the dome pressure. Finally, they observed a sharp decrease in filler pipe pressure followed by a pressure rise to a value greater than before the drop at click-off. This occurred in both NSO and PSO events.

Mathematical models presented by Lockhart (1997) and Reddy (2010) were able to estimate refueling vapor generation [12, 21]. Vapor generation is the amount of HC vapor that must be displaced while refueling, in g/gal. Lockhart presents and evaluates three different models, including an empirical regression presented in the work of Cingle and McClement [18]. Reddy presents an empirically derived model. They also include the effects of a bottom fill (no spray) versus a top fill (fuel is sprayed into the headspace) and mechanical seal (no air entrainment) versus a liquid or dynamic seal (allows fresh air entrainment). Both compare to a variety of test data, including the study of Cingle and McClement. Lockhart finds that each

model presented provides reasonable estimates of vapor generation. Reddy's model has an R^2 value of 0.96 when compared with the Cingle and McClement data. However, these models did not predict the amount of vapor leaving the refueling system, the emissions value.

Lavoie et al. created a fuel vapor system model (FVSMOD) to simulate each of the EPA evaporative emissions tests in 1998 [22]. The mathematical model included an empirically derived equation to account for weathering, changing fuel composition, effects on vapor pressure. They also included a one-dimensional absorptive and diffusive bed model for canister loading and purging. For refueling emissions, the model is able to predict trends but not entirely explain experimental data. The authors cite the assumption of vapor/liquid equilibrium as a probable reason for the discrepancy. Not included in the model is the VRL and the emissions escaping out of the filler pipe entrance.

Simple, 0D models have proven useful for simulating certain aspects of the refueling process. Fackrell et al. (2003) presented a lumped-parameter model of the refueling system [23]. They simplified the system into four rectangular control volumes (annular area around liquid from fuel nozzle, collection of liquid fuel at bottom of filler pipe, collection of liquid in the tank, and headspace vapors) with four valves (opening of filler pipe around fuel nozzle, filler pipe into the tank, VRL, and canister). Each control volume and valve had its own equations, interacting with the other zones. They also include choked flow effects in the canister and VRL. Including those effects allowed the model to correlate with experimental PSO results. They also show agreement in the time taken to fill the tank. However, the model only reached fair agreement with system pressures, in both NSO and PSO cases.

Sinha et al. (1998) investigated the process of early click-off with simulations [24]. They identified the general process and important events/factors that lead to this phenomenon.

However, they note that approximations were used in place of a variety of missing data. Their simulations do not reflect the entire refueling process or the entire refueling system.

The work of Sinha et al. is also useful for its description of the tank pressure-time profile during refueling. Figure 4 shows the general profile. This begins with an initial rise in pressure as the fuel reaches the tank. A maximum value is reached before falling to a lower value. This is marked as Phase I in the figure. A steady pressure is reached as the air/vapor mixture vents through the VRL and canister line. This is the longest portion of the fill and is noted as Phase II in the figure. Finally, when the tank is full and both vent paths are closed, the headspace gas is compressed and the pressure rises to a significant peak. During this pressure rise, the fuel column in the filler pipe builds until it reaches the nozzle and triggers the automatic shutoff mechanism. The tank pressure then is gradually relieved back to atmospheric conditions. This is Phase III in the figure. This characteristic profile will be observed in the current work.

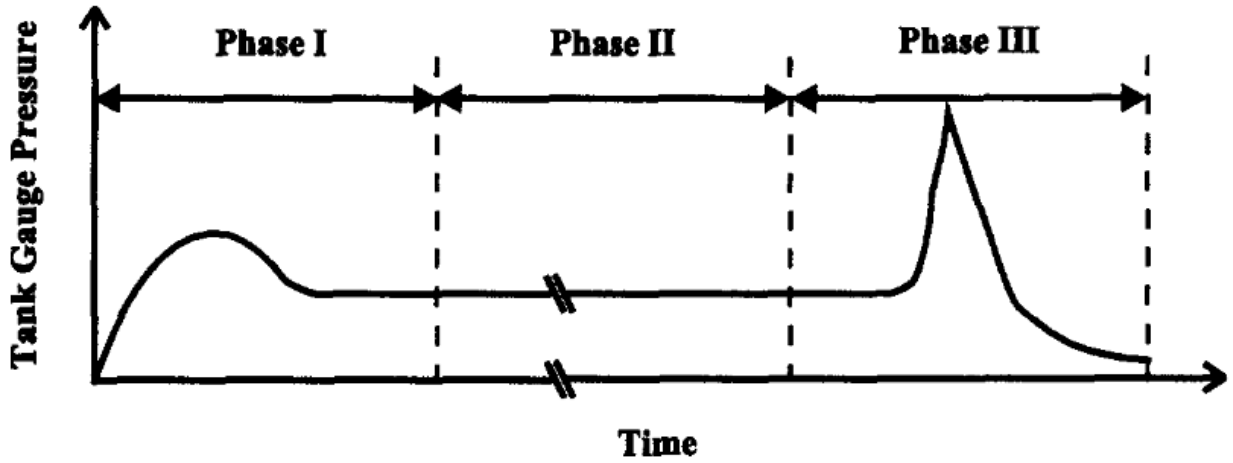

Figure 4: The general tank pressure-time profile during the refueling process [23].

2.4 Summary of CFD Approach

As this work has supported CFD development, a brief explanation of the CFD method is presented here. The simulations were carried out using the commercial software STAR-CCM+ [25]. The flow in automotive refueling systems is highly turbulent and may be considered as

being composed of different phases, with air, HC vapor, and liquid fuel as the separate phases [15, 26]. The Volume of Fluid (VOF) method has often been used to study this phenomenon; e.g. studies by Banerjee and Dake [13, 14, 17]. Unlike the Eulerian approach that solves conservation equations for each phase, VOF solves one set of equations that is shared by the multiple phases. Thus, it is less computationally expensive.

VOF keeps track of the volume fraction of each phase at each point in the simulation domain. The volume fraction of each phase in each cell is determined by a simple equation:

$$a_i = \frac{V_i}{V} \quad \text{Eq. 1}$$

where a_i is the volume fraction of phase i, V_i is the volume of phase i, and V is the total volume of the cell. The volume fractions of all phases in a cell must add to one:

$$\sum_{i=1}^{N} a_i = 1 \quad \text{Eq. 2}$$

where N is the total number of phases. An a_i of one indicates the cell is completely occupied by phase i, zero indicates the cell is completely void of the phase, and values in between indicate an interface between phases.

When multiple fluids are in the same cell, they are treated as a mixture. The properties of that mixture are then a volume fraction weighted summation of the properties of the constituent fluids:

$$\rho = \sum_i \rho_i a_i \quad \text{Eq. 3}$$

$$\mu = \sum_i \mu_i a_i \quad \text{Eq. 4}$$

$$C_p = \sum_i \frac{C_{p_i} \rho_i}{\rho} a_i \quad \text{Eq. 5}$$

In the above equations, ρ_i is the density, μ_i is the dynamic viscosity, and C_{p_i} is the specific heat of phase i. The phase mass conservations equation is:

$$\frac{\partial}{\partial t}\int_V a_i dV + \oint_A a_i v \cdot da = \int_V \left(S_{a_i} - \frac{a_i D\rho_i}{\rho_i Dt}\right) dV \quad \text{Eq. 6}$$

where a is the surface area vector, v is the velocity, S_{a_i} is a user-defined source term for phase i, and $D\rho_i/Dt$ is the material or Lagrangian derivative of the phase densities ρ_i. The source term allows inclusion of phase change. The source term in STAR-CCM+ can be a constant value, a user-defined field function, or by incorporating condensation-evaporation modeling.

Flow in the refueling system is highly turbulent. In the filler pipe, the Reynolds numbers range from about 10,000 to 40,000 with the flow rates considered. The K-ε turbulence model was used in simulations, as suggested by previous work [16].

2.5 Summary of Previous Work and Motivation for Current Study

Several gaps are found in the literature. These gaps have motivated the current study. The current work seeks to address them.

- A CFD model of a production refueling system capable of estimating flow parameters and emissions values without experimental input is missing. Many models are capable of simulating some aspects, but no model in the literature has predictive capability to be confidently utilized in the vehicle design cycle.
- CFD predictions of emissions values in an ORVR system are not found. Though vapor generation models exist, the actual amount of vapors escaping to the environment has not yet been predicted. Geometry considerations and CFD are needed for this.
- Real-time data of refueling emissions. This would provide understanding of the events that contribute to HC emissions. Such data would also allow simplification of CFD emissions estimates by simulating only the events of greatest importance.

3. Experimental Methods

3.1 Refueling System

The refueling system used in this study comes from the 2016 Honda Pilot. All components were provided by Honda R&D Americas, Inc. The CAD geometry of the same system design was used to develop the fluid domain for the CFD model. Figure 5 is a view of the CAD model of the system. Annotations in the figure point to key components. The experimental rig was constructed to match the configuration of the system in the vehicle.

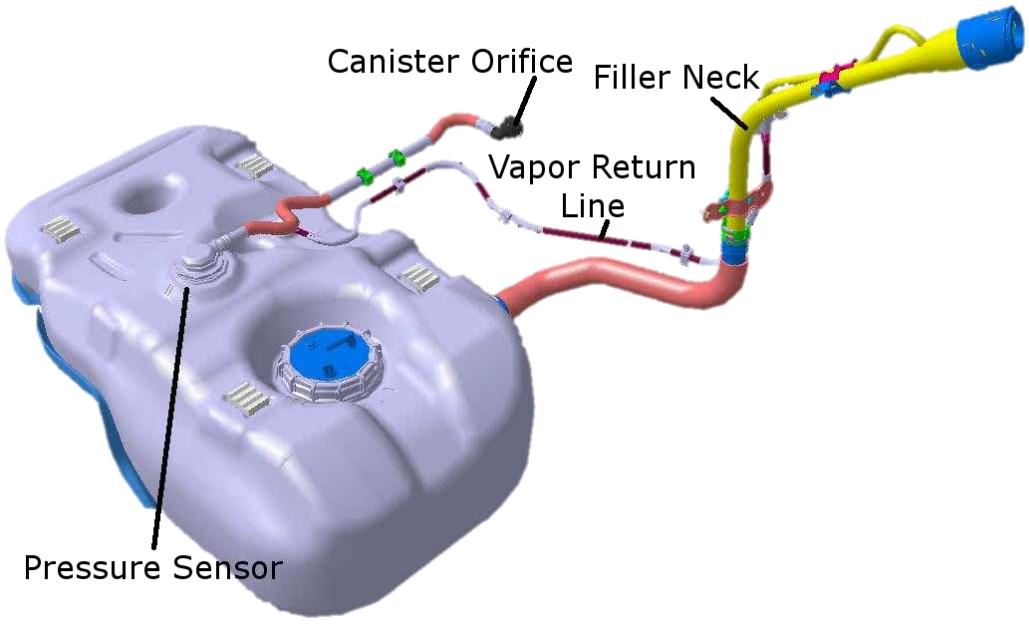

Figure 5: CAD model of the refueling system with key components identified.

Figure 5 labels a "Canister Orifice." For Phase I of this study, where evaporation was neglected, an orifice was placed where the canister would be connected. This mimicked the pressure versus flow characteristics of the canister, allowing for the same refueling system flow characteristics (discussed in more detail later). For Phase II, this was replaced with the activated-carbon canister used in the production system. Figure 6 shows this activated-carbon canister.

Figure 6: Activated-carbon canister used in the study.

3.2 Phase I – Support for CFD Model without Evaporation/Condensation

3.2.1 Fuel and Fuel Delivery

For Phase I, Stoddard solvent was used. In the initial trial of the full system model, it was desired to neglect evaporation and condensation. The flow is highly turbulent, with Reynolds numbers greater than 10,000 for fuel flow of 4 GPM. Furthermore, the simulation is transient with flow start and final pressure and fuel column building effects. The turbulent flow prediction was to be validated without introducing unintended uncertainty while attempting to predict evaporation/condensation. There should be negligible evaporation in the experiments to allow comparison with such a model. Thus, Stoddard solvent was chosen as it has very low vapor

pressure. This was used in the full tank filling tests to validate the initial model. Properties of Stoddard solvent were also used in simulations. Table 1 presents some properties of Stoddard solvent compared with the EPA test gasoline (indolene) [3]. RVP for Stoddard solvent is 2% of the value for indolene, indicating minimal evaporation. For reference, the RVP of water is approximately 0.95 psi. Density values are similar between indolene and Stoddard solvent, matching within 4%. The dynamic viscosities are dissimilar, but the difference is accounted for by using Stoddard solvent properties in simulations, thus allowing for direct comparison with experiments.

Table 1: Some properties of Stoddard solvent and indolene.

	RVP (psi)	Dynamic Viscosity @ 25°C (mPa*s)	Density @ 25°C (g/cm^3)
Indolene	9	0.413	0.749
Stoddard solvent	0.22	0.905	0.778

Fuel flow was provided by a Webber Engineering and Manufacturing, Inc. 50300-114M fuel cart. The unit was modified to achieve higher dispensing rates by bypassing the flow controller and conditioning systems. When in use, the conditioning system allows fuel to be cooled as needed. This function was not needed for Phase I. By bypassing the flow controller and conditioner, fuel flow rates of 16.5 GPM were achieved with Stoddard solvent. Note that bypassing the flow controller also included bypassing fuel cart gauges, including the dispensing counter. Thus, the exact amount of fuel dispensed in each test is not known, but could be estimated by the transient flow rate measurement (described below).

An OPW 11B fuel nozzle was used in all experiments. This nozzle is specified for the EPA refueling tests [3] and is the commonly used at refueling stations in the United States. As

noted in the Literature Review of Chapter 2, this was one of the nozzles studied by Dake et al. [17]. Figure 7 shows the difference in the outlet geometry of the OPW 11B nozzle as compared to the Husky X1 nozzle.

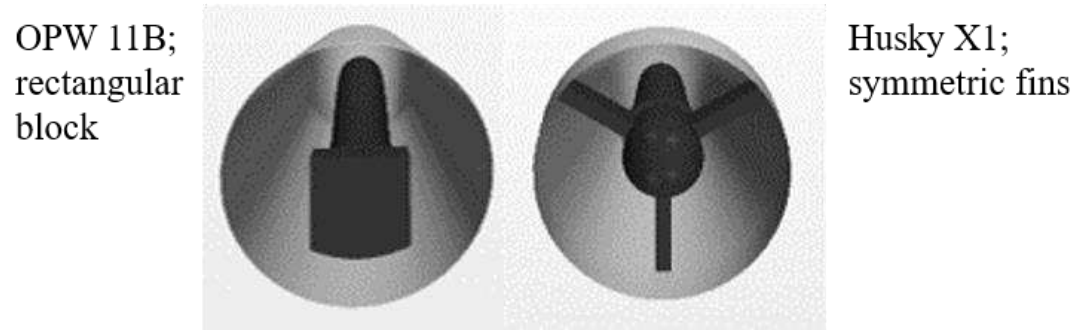

Figure 7: Comparison of the outlet geometries of the OPW 11B and Husky X1 nozzles.

As the flow controller was bypassed, a new solution for flow control was needed. An Omega digital flow meter and a ball valve were placed in the fuel dispensing hose, just upstream of the fuel nozzle. Figure 8 pictures these components. To set a flow rate, the nozzle is placed in the top of the barrel from which the fuel is pumped, recirculating the fluid. With the fuel cart set to dispense, the nozzle trigger is set to the fully open position on the rack. Then the ball valve is adjusted until the Omega flow meter reads the desired flow rate. The ball valve is left in this position while testing at that flow rate.

Figure 8: Photograph of the ball valve and Omega digital flow meter.

For real-time monitoring and recording of fuel flow rate, a Flow Technology, Inc. (FTI) turbine flow meter was used (model number FT-12NENS-LEA-3). The standard range is 2-20 GPM. The frequency of the device is proportional to flow rate; it sends 6000 magnetic pulses per gallon flowing through the turbine. Thus, the frequency at the maximum of the unit's range is 2000 Hz. The FTI flow meter was installed just after the fuel cart pump. This was then followed by the fuel hose and nozzle.

A diaphragm pump was used to empty the tank after each experiment. The unit was a Nitrile model 17150500. It pulled the fuel from a bulkhead fitting at the bottom of the tank. This was closed with a ball valve during testing.

3.2.2 Data Acquisition

The pressure sensor used for the experiments was a silicone diaphragm type transducer. The operating range was -6.67 to 6.67 kPa gauge pressure. Two thermocouples were used, a K-

type and a T-type. The T-type thermocouple recorded ambient temperature. The K-type thermocouple was placed in the fuel line just upstream of the nozzle. This recorded fuel temperature while dispensing and was used to identify poor tests where the pump heated the Stoddard solvent excessively.

Two National Instruments DAQ cartridges were used, with model numbers NI 9205 and NI 9211. NI 9205 collected raw voltage signals from the pressure transducer and turbine flow meter. NI 9211 was used for thermocouples. LabVIEW 2015 by National Instruments was used to gather and record data from the various sensors [27]. This included the pressure transducer, thermocouples, and the FTI turbine flow meter.

Figure 9 shows the flow of fuel and data through the test setup. The schematic gives an overall visual of the equipment used for Phase I non-evaporative filling tests.

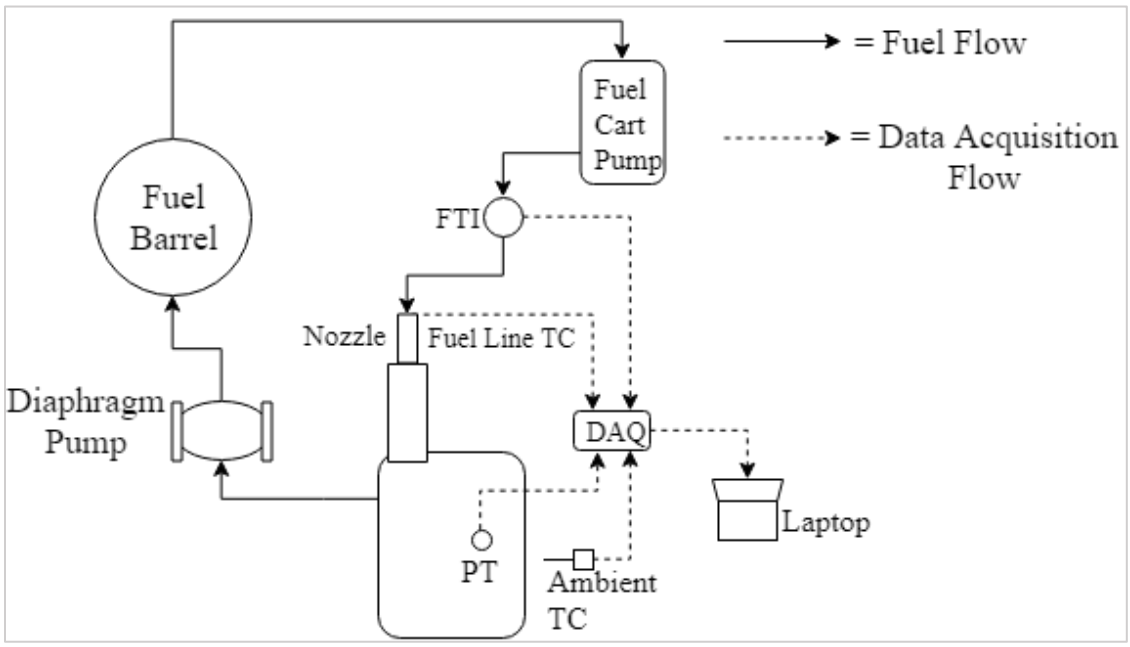

Figure 9: Schematic of the fuel and data flow for Phase I non-evaporative filling tests. TC stands for Thermocouple and PT stands for Pressure Transducer.

3.2.3 Procedure Description

3.2.3.1 Canister and VRL Characterization

Characterizing the canister orifice and VRL boundary conditions for CFD was done with simple flow bench experiments. The canister orifice data verified the CFD model flow predictions through that boundary. The VRL was characterized to create a function or table to govern flow through two boundaries: an outlet from the tank and an inlet to the fuel filler pipe. Not meshing the complex VRL geometry would save significant computational time. A Mass Flow Controller (MFC) was used to set the flow rate of air in Standard Liters Per Minute (SLPM), which was provided by the building compressed air supply. For the MFC, standard conditions were defined as 25°C and 1 atm pressure. The air went through a straight pipe section of approximately six feet and then through the respective component. Figure 10 is a schematic of the test setup. Either a manometer or a pressure transducer, the same type as the unit in the tank, measured the differential pressure across the component. The manometer was used for differential pressures ≤ 1200 Pa, as this was its range.

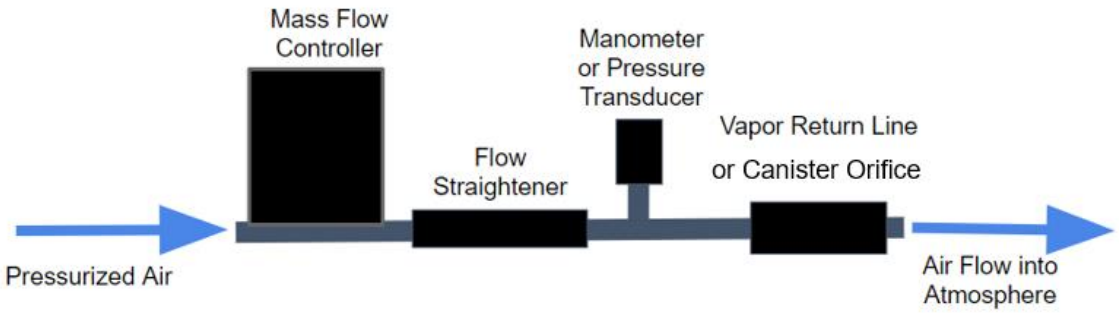

Figure 10: Schematic of the flow bench experiment used to characterize the canister orifice and the VRL.

3.2.3.2 Non-evaporative Full Tank Filling Tests

The tank was filled at least three times at the following flow rates: 4, 10, and 14 GPM. Most gasoline station pumps flow around 10 GPM, but 4 GPM may be used in EPA testing [3]. Flow at 14 GPM represents an extreme case to ensure correct operation of the refueling system.

The CFD model was to be validated with all three flow rates. The tank was empty prior to each test. Prior to insertion of the nozzle into the fuel filler pipe, the Stoddard solvent was dispensed into its own barrel to minimize pump startup effects and ensure the correct flow rate. The fuel nozzle was fully inserted with no rotation (the symmetric plane of the handle was perpendicular to the ground). Fuel was dispensed until automatic shutoff occurred. The test system did not have any cases of early click-off. Tank pressure, by the canister inlet, was recorded for each test. This was the main point of correlation with CFD. As a qualitative metric, high speed images of the flow in the filler pipe were captured using a translucent filler pipe of the same design as the production unit. The images and pressure and flow data were all synced in post-processing. Figure 11 shows a photo of the translucent filler pipe.

Figure 11: Translucent filler pipe used for high-speed imaging of Stoddard solvent flow in Phase I.

3.3 Phase II – Investigation of Refueling System Emission Dynamics

3.3.1 Fuels and Fuel Delivery

Indolene was used in Phase II. As specified in Chapter 2, indolene is the gasoline designated by the EPA for refueling emissions tests [3]. The same fuel cart was used as in Phase I. The fuel conditioner was incorporated in Phase II to allow fuel cooling; however, the fuel cart flow controller remained bypassed. This setup allowed for a maximum flow rate of 11.5 GPM with indolene at room temperature. As Phase II tests were performed at approximately 9.8 GPM, the maximum flow rate was acceptable. The conditioning unit on the fuel cart was able to lower fuel temperature to approximately 50^{o}F.

The same FTI flow meter was used in this phase as in Phase I. However, instead of the fuel hose coming immediately downstream of the FTI unit, the flow meter was followed by the conditioner. Emptying the tank was accomplished with the same diaphragm pump and bulkhead fitting.

3.3.2 Data Acquisition

The pressure sensor and thermocouples from Phase I were also incorporated in Phase II. Two additional K-type thermocouples were placed in the tank, one near the bottom and one near the top. The bottom thermocouple was placed such that it would capture the temperature of the pre-fill fuel. The top sensor recorded the temperature of the gases present in the headspace for the majority of the fill, until the fuel level reached the thermocouple. Figure 12 shows the locations of the pressure transducer and the tank thermocouples. The location of the fuel line thermocouple was too far downstream to monitor the fuel temperature as it was being cooled. Instead, the fuel temperature during conditioning was estimated from the water (coolant)

temperature gauge on the fuel cart. Then the actual fuel temperature would be captured while dispensing.

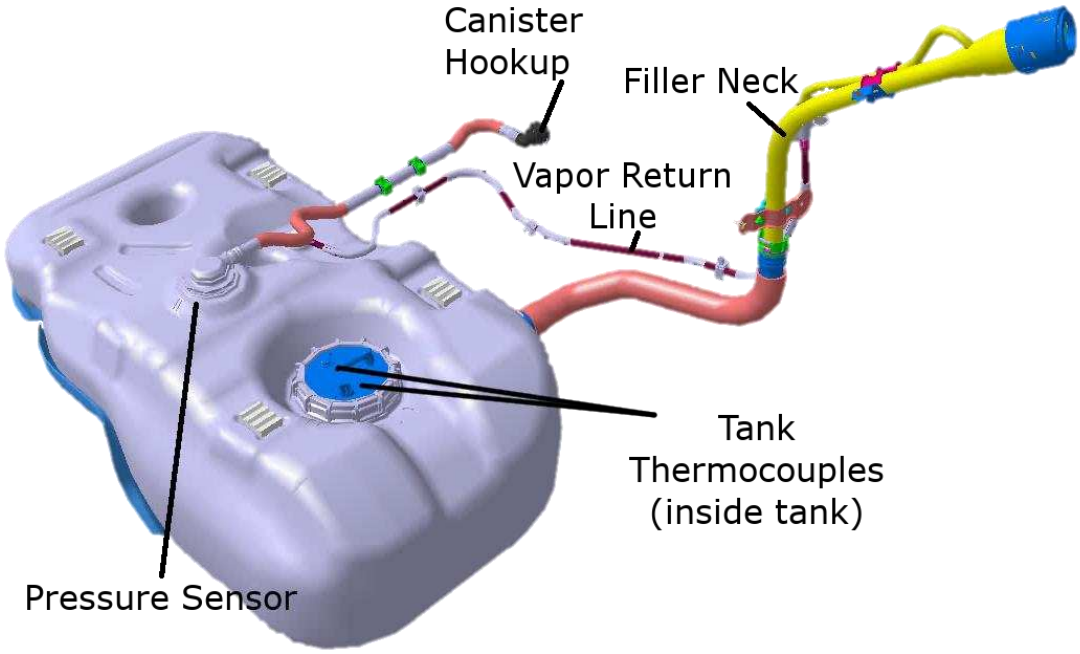

Figure 12: CAD model of refueling system with tank thermocouple locations identified.

The Phase I DAQ units were used here, incorporating the additional thermocouples. The LabVIEW Virtual Instrument (VI) was modified to record the additional thermocouple data.

A FLIR G300a camera was used for infrared (IR) videos to monitor fuel vapor emissions during fueling. This was focused on the capless module, which is the entrance into the fuel filler pipe, and the nozzle. FLIR IR Camera Player version 2.3.5 was used to record the videos to a laptop.

A FIDAMAT 6 unit produced by Siemens was used for HC concentration measurement. It has a calibrated range up to 5000 ppm. Maximum measurement frequency is 5 Hz, but this was set to 1 Hz for the current work.

Not all of the emissions were captured and measured, as they would be in a SHED during the EPA test. Instead, emissions were sampled from a single sampling point. The point just on top of the nozzle and nearly flush with the capless module was chosen as the sampling point,

which may also be referred to as the probe. The end of a 1/4” tube was placed here. Figure 13 is a simple schematic of this setup and Figure 14 shows a photo of the probe location taken from IR video. The tubing was connected to a heated line feeding into the FID. The FID and line had internal pumping to pull sample continuously at approximately 10 LPM. Though not all vapors were captured, the sample collected at this point would have concentrations proportional to the total HC emissions.

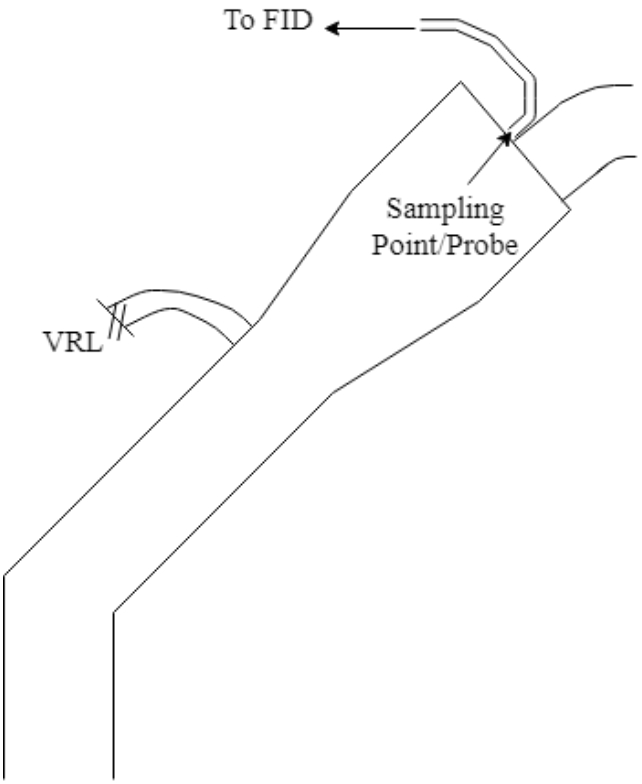

Figure 13: Schematic showing the sampling point/probe.

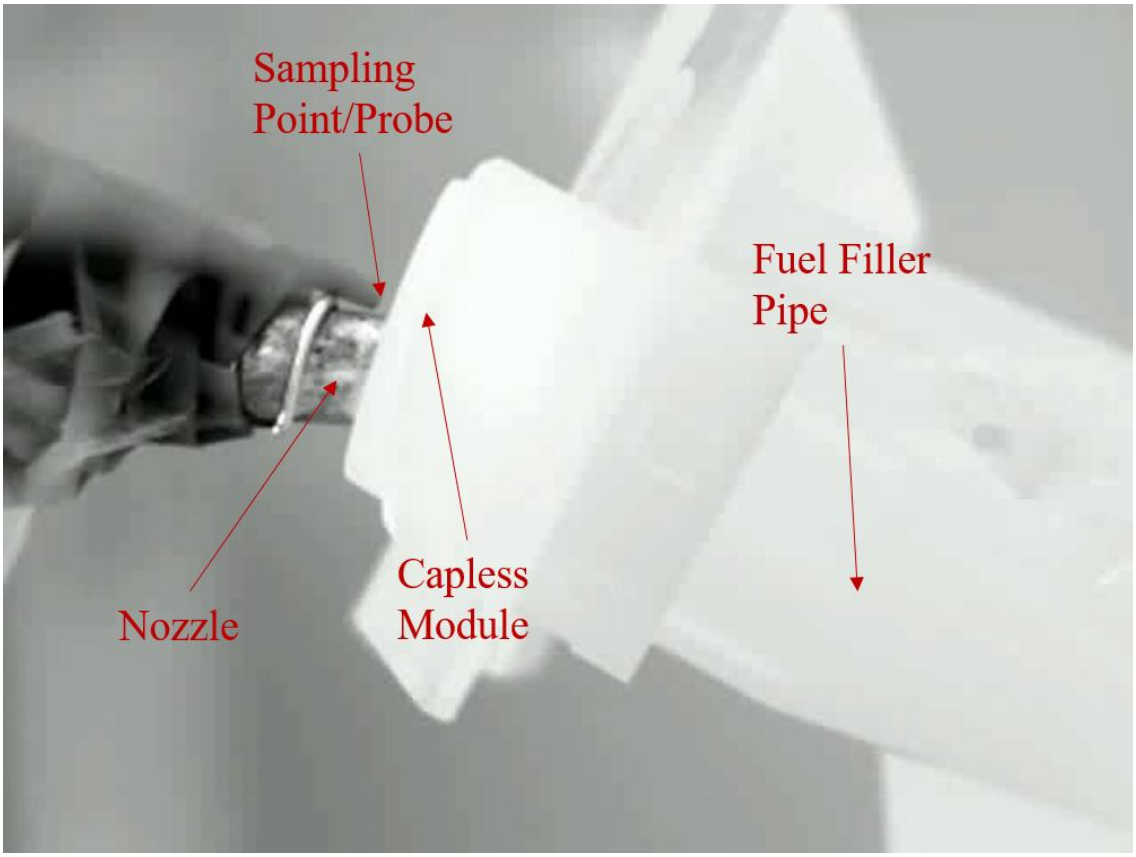

Figure 14: Photo of probe location from IR video

The pressure created by the sampling system likely pulls additional vapors from the filler pipe. The system pulls about 10 LPM. The inside diameter of the sampling line is approximately 4.21 mm. Thus, the velocity is about 12 m/s at the probe. The Bernoulli equation was used to estimate pressure drop from quiescent air to inside the sampling line:

$$P_1 + {}^1\!/_2\,\rho v_1^2 + \rho g h_1 = P_2 + {}^1\!/_2\,\rho v_2^2 + \rho g h_2 \qquad \text{Eq. 7}$$

In Eq. 7, P is the pressure, ρ is the density, v is the velocity, g is the acceleration due to gravity, and h is the height. Subscript 1 denotes the quiescent environment and subscript 2 denotes the probe location. Assuming no change in height and v_1 equal to zero, the pressure drop (P_1-P_2) is estimated to be 87.8 Pa. This pressure could pull additional vapors from the filler pipe and lead to overestimating the concentration of vapors in normal operation (without sampling instrumentation).

However, as sampling line flow is constant, the current setup is sufficient for comparison of various cases. This allows for trends to be seen as components are changed (explained in more detail later). Such data will allow comparison with CFD model results to determine if the same trends can be captured in simulation. Finally, the current setup allows investigation of emissions timing. This is critical to discovering assumptions to simplify the CFD.

If the exact HC concentration were desired, then the sampling system would have to be modified in some manner to negate the disturbance of vapors in the filler pipe. For example, a lower sampling flow rate may be used. A larger diameter sampling line might be used to decrease the velocity and pressure drop. Or dilution could be incorporated, pulling less flow from the sampling area by providing a known flow of an inert gas downstream.

As there was great length of transfer line, there was a time delay between vapors entering the sampling tube and being detected at the FID. As the length of heated FID line was unknown, the transfer time could not be calculated. Instead, the transfer time was tested by suddenly moving the probe over a beaker of indolene and holding it there for 3 to 5 seconds. The time of the movement was recorded. Then the point in the FID data where the concentration value began to increase was taken as the point when the vapors reached the FID. The difference from the time of movement to the time of concentration increase was the transfer time. This was used to shift timing of FID data to match other data (pressure, temperature, flow). Figure 15 shows the FID trace from the transfer time testing. HC concentration is shown in parts per million (ppm). After five trials, the average transfer time was found to be 27 seconds with a standard deviation of 0.71 second.

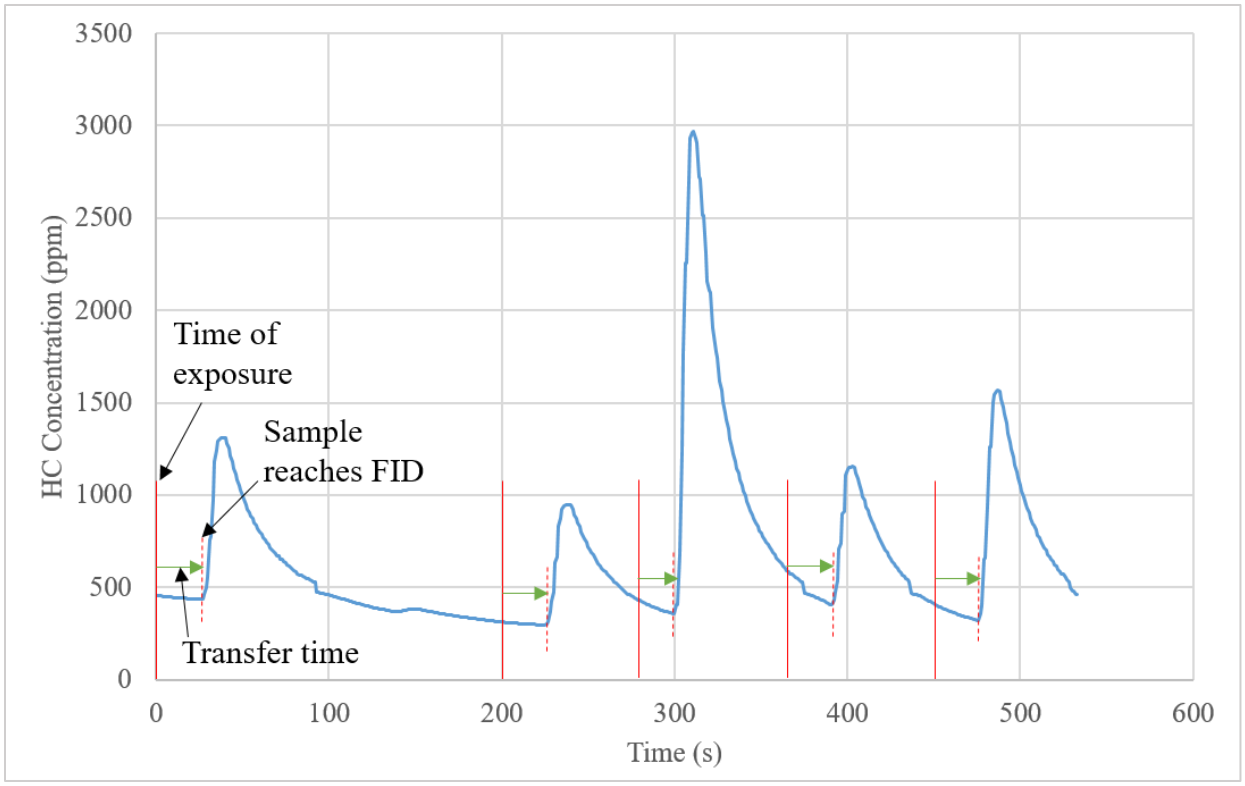

Figure 15: FID trace from the transfer time test.

With high HC concentration in headspace gases (around 40-60%), dilution was thought to be necessary. However, after preliminary testing without dilution, the FID reading did not surpass the maximum. This is likely due to natural dilution with ambient air. Headspace gases interact with air being entrained into the filler pipe and a brief space of air outside the filler pipe before reaching the probe.

Figure 16 is a schematic of the flow of fuel, data, and emissions in the Phase II experiments. Compared with Figure 9, the schematic of Phase I flow, the addition of tank thermocouples, fuel conditioner, and emissions sampling equipment may be noted.

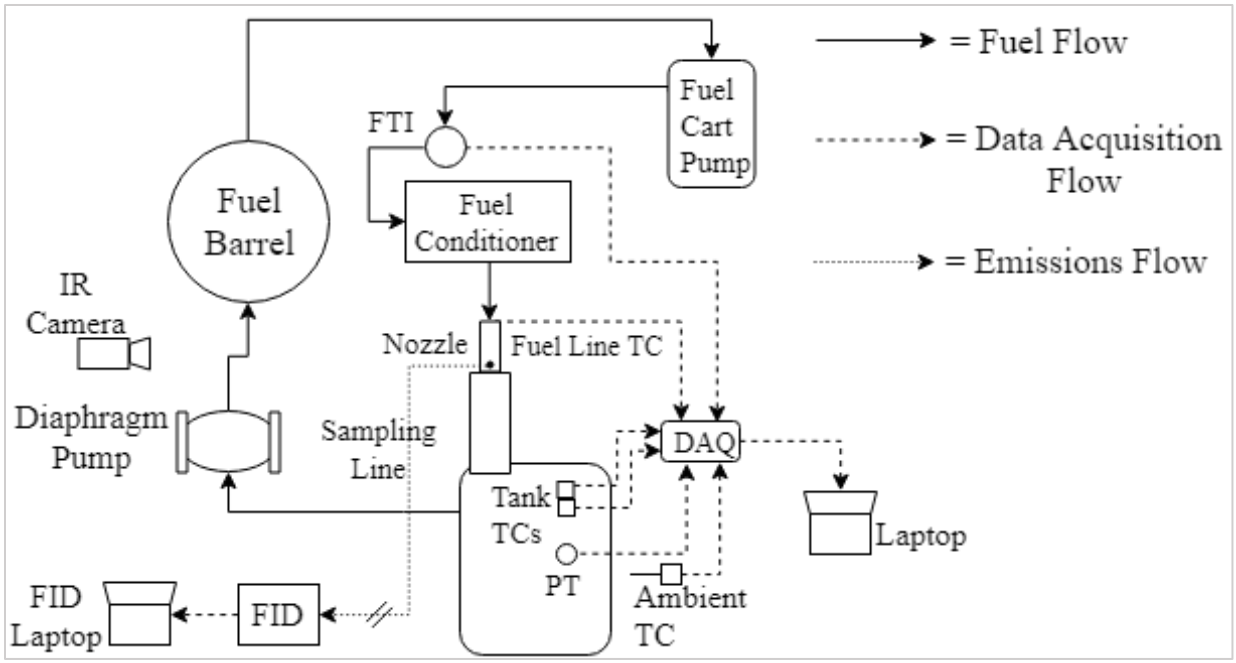

Figure 16: Schematic of Phase II experiment fuel, emissions, and data flow. TC stands for Thermocouple and PT stands for Pressure Transducer.

3.3.3 Procedure Description

Phase II tests were performed to investigate the emissions from the refueling system. First, the timing of emissions were to be observed. Such investigation has not been performed before. SHED experiments cannot reveal the transience of vapors escaping the refueling system. If events critical to emissions can be determined, then simplifications can be made in the CFD model, reducing computational time. Perhaps only the critical events need to be simulated, ignoring the rest of the refueling process.

In addition, various combinations of vapor path pressure drops, or backpressures, are tested. The hypothesis was that as the pressure drop of one path increases, less of the headspace mixture will take that path, as it is more resistive to flow. Thus, more headspace gases, and consequently more vapors, would take the other path. As VRL backpressure increases, more vapors should go through the canister. This should be observed in the mass gain of the canister, which is the mass of HCs adsorbed during the test. However, as canister backpressure increases,

more vapors would travel through the VRL. More vapors introduced to the filler pipe should lead to more emissions, and this should be observed in higher HC concentrations at the probe. The hypothesis was to be confirmed with Phase II tests.

Discovery of possible non-linear relationships also motivated Phase II experiments. For example, the effect of VRL backpressure on air entrainment is unknown. Though a higher backpressure may lead to less vapors traveling through the VRL, this may also lead to greater air entrainment and more vapor generation, leading to increased emissions. Testing various vapor path pressure drops also allows investigation of the interaction of the two paths. The result of increasing or decreasing the backpressure of both paths was unknown. The effect may be different than the effect of changing a single vapor path.

Finally, datasets collected with testing of the various pressure drops will allow validation of the CFD model. Simulations should be able to distinguish changes in emissions and canister mass gain due to the differing vapor path backpressures. The data will also validate if estimates from simulating only portions of the fill are accurate.

Phase II tests were conducted similarly to the EPA refueling emissions test. The canister was weighed and set aside. The tank was pre-filled for 12 seconds at 9.8 ± 0.2 GPM, filling ~10% of the tank volume. Then the fuel was cooled and the tank heated until the difference between the pre-fill and fuel temperatures was between 10 and 13°F. This temperature difference will be referred to as DeltaT. This DeltaT range was set to mimic the EPA test constraints, where the dispensed fuel is set at 67°F and the pre-fill is at 80°F. The lower end of the DeltaT range was set to account for the uncertainty in dispensed fuel temperature. As noted previously, the dispensed fuel temperature while cooling was estimated as the coolant temperature. Thus, the DeltaT was estimated using the coolant temperature and the DeltaT range ensured that the 13°F

upper value was not exceeded. No soak temperature or time was specified as ambient temperature was not controlled. The time between pre-fill and test start was whatever time passed for DeltaT to reach the specified range. Before each test, a sample of indolene was taken to measure the RVP value for the test. The canister was installed just prior to the test; it was not present during the pre-fill or temperature conditioning stages. The nozzle was inserted into the filler pipe (with no rotation) and allowed to sit for about two minutes. As the FID data was recorded on a separate laptop, the time of insertion was noted. A stopwatch was used to keep track of the timing of various events in the LabVIEW data. Flow was then started at the previously set flow rate of 9.8 ± 0.2 GPM. In the IR videos, a hand wave just prior to pulling the nozzle trigger indicated that flow was about to start. Indolene was dispensed until automatic shutoff; no cases experienced early click-off. After shutoff, data was recorded for an additional minute. The canister was weighed again and then purged. The tank was drained and was then ready for the pre-fill for the next test.

Tests were performed with three canister backpressures and three VRL backpressures. Table 2 shows the test matrix of nine combinations. The nomenclature presented will be used to identify the cases in Chapter 4. Pressures listed are the pressure drops across the components while 10 SLPM of air is flowed through. Standard conditions here are defined as 70ºF (21.1ºC) and 1 atm pressure; a mass flow meter, not the MFC from the Phase I flow bench tests, was used for these pressure measurements. Only a portion of the VRL was changed, not the entire line. Thus, the backpressures listed are for the changed component. VRL 1 is a short length of tubing, approximately 3 inches. The pressure drop for this component was not measured but calculated as a major pressure loss. Note that the canister components have two pressures listed. This is

because two different canisters were used in testing, to allow purging of one during testing with another. Both are the same design but have slightly different pressure drops.

Table 2: Test matrix of component combinations. Pressure drops shown are measured with 10 SLPM air flow.

	VRL 1 (1.3 Pa)	**VRL 2 (255.7 Pa)**	**VRL 3 (827.5 Pa)**
Canister 1 (123.3/141.3 Pa)	C1V1	C1V2	C1V3
Canister 2 (219.9/239.8 Pa)	C2V1	C2V2	C2V3
Canister 3 (331.4/357.3 Pa)	C3V1	C3V2	C3V3

4. Results and Discussion

4.1 Phase I – Support for CFD Model without Evaporation/Condensation

4.1.1 Boundary Characterization

Simple flow bench experiments were carried out for the standard VRL and the canister orifice. Shown first are the results of the canister characterization. Figure 17 shows the graph of pressure versus flow. Because the canister orifice is not an intricate geometry, it was modeled directly in the CFD. The characterization data was used to confirm accuracy of the model flow predictions. Figure 15 also displays simulation data points and polynomial fit.

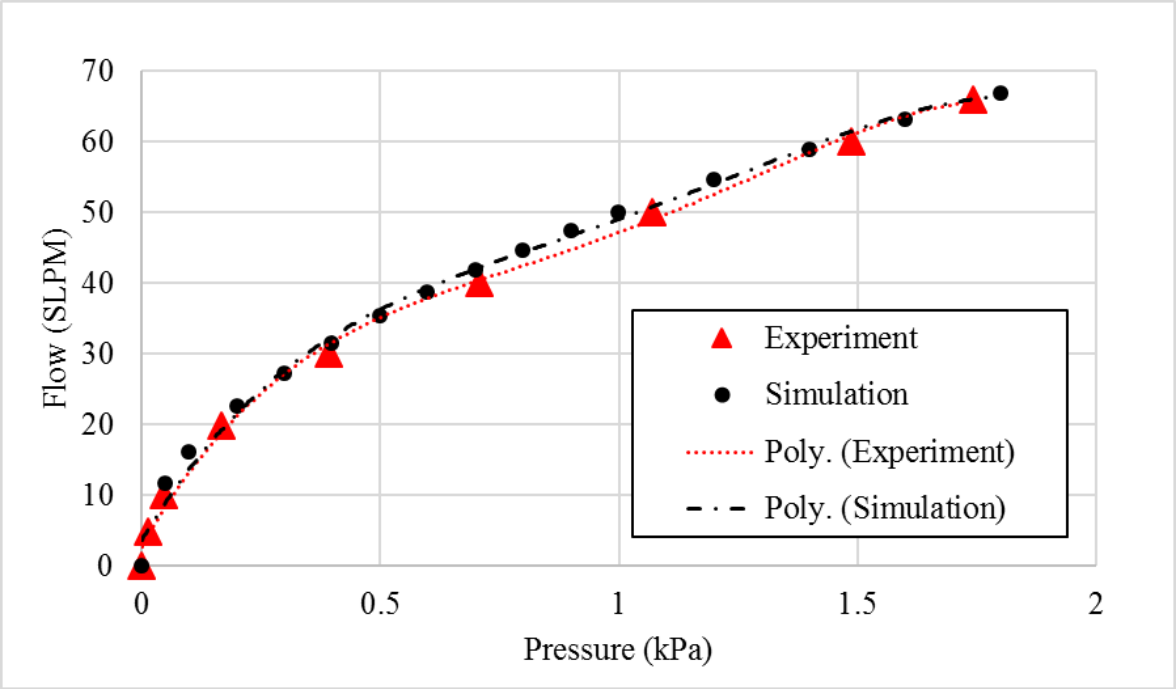

Figure 17: Flow bench results for the canister orifice and line, both data points and polynomial fits.

Figure 18 shows the flow bench test results for the VRL. These were used to create a polynomial function. Thus, the VRL did not need to be meshed in CFD. Instead, it was modeled as an outlet from the tank and an inlet to the filler pipe, with the function governing the flow through those boundaries.

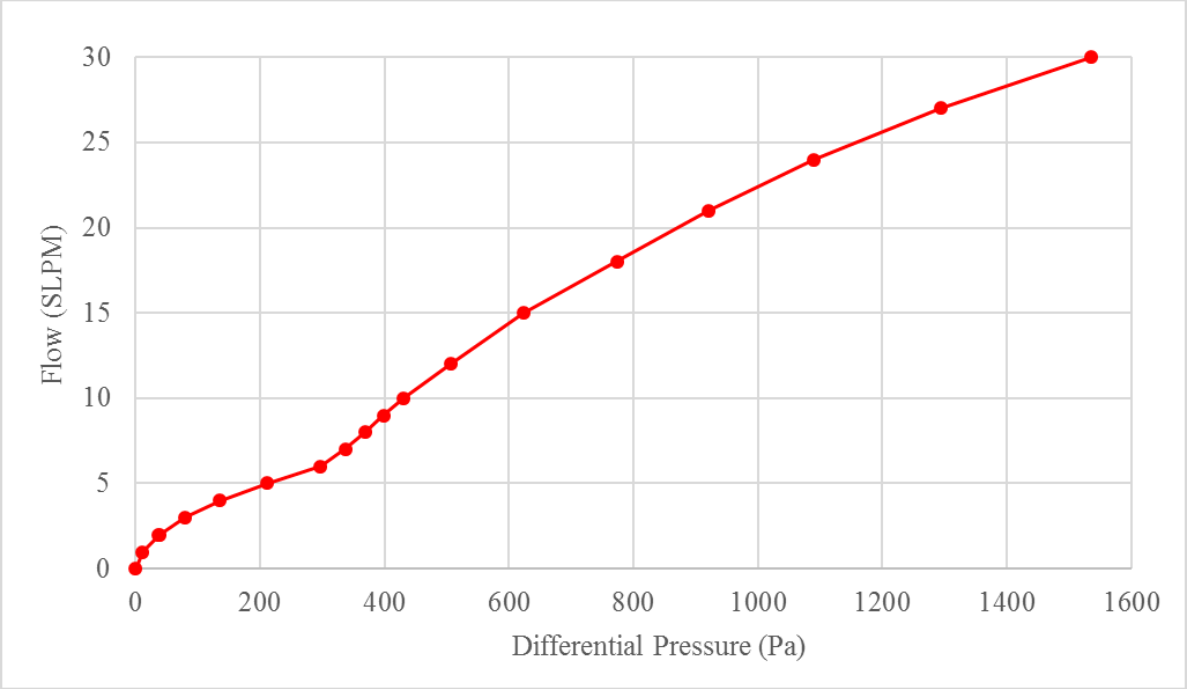

Figure 18: Flow bench results for the VRL.

4.1.2 Non-evaporative Filling Tests

Filling tests were performed at 4, 10, and 14 GPM. The averaged pressure traces are shown in Figure 19. These were taken with the sensor by the canister inlet. Pressure was monitored at the same place in CFD. The pressure trace from simulation of the 14 GPM case is also included in Figure 19. More details on the model development may be found in a 2019 SAE technical paper [28]. The figure is also labeled with important fill events.

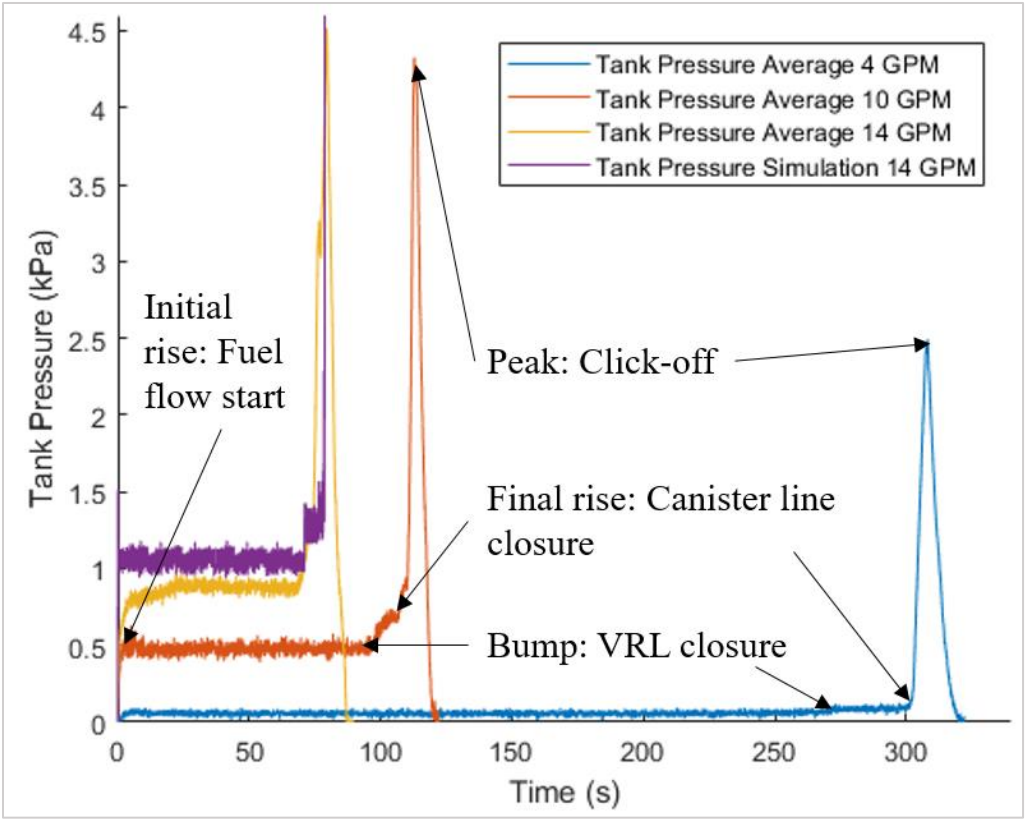

Figure 19: Averaged pressure traces from experiments and the 14 GPM simulation trace, performed with Stoddard solvent. Key events are labeled.

The pressure profiles follow the general trend stated by Sinha et al. [24] except that there is no maximum noted in phase I (see Figure 4). Instead, the pressure steadily builds up to the steady state value. This is likely due to the low volatility of Stoddard solvent compared to gasoline. The rapid evaporation of gasoline entering an empty tank greatly affects the initial pressure.

Pressures from the steady state portion (phase II of the fill) were averaged and compared with CFD results. These were taken at times after the initial pressure rise but before the slight pressure bump. Though not noted in the literature, this slight bump prior to the pressure spike is due to the VRL being covered by fuel. Thus, the canister becomes the only escape for headspace gases for the last portion of the fill causing the pressure to slightly rise in the tank. Figure 20 displays a bar chart comparing average steady state pressures.

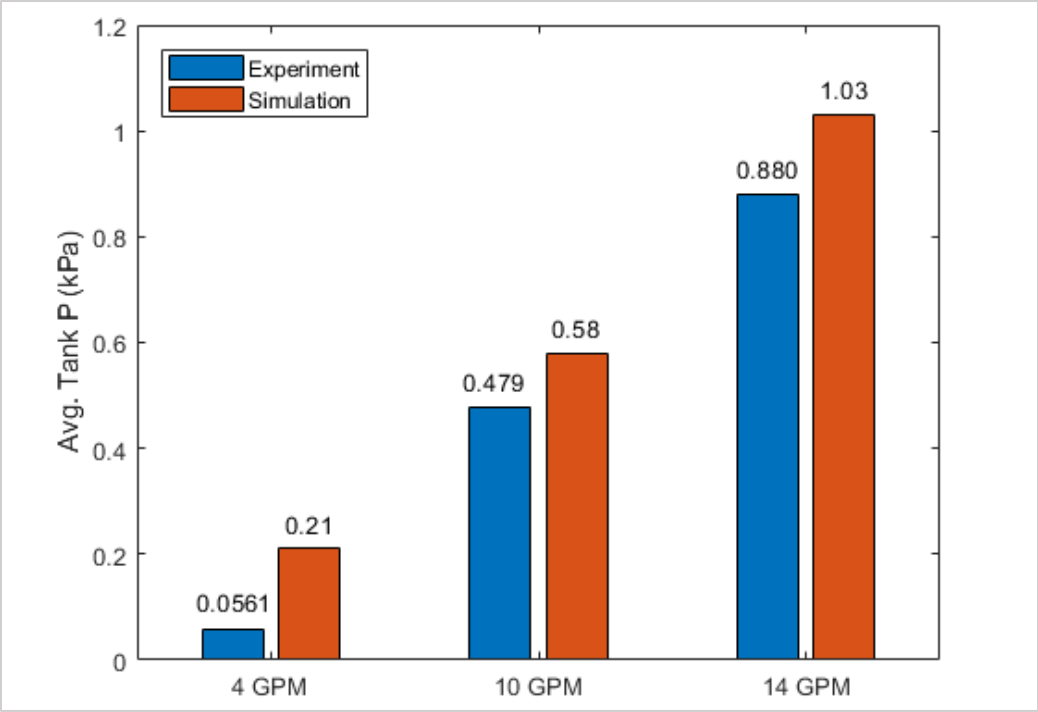

Figure 20: Bar chart comparison of steady state pressures in experiment and simulation.

Steady state pressure increases with fuel flow rate. This agrees with previous work [20]. The same trend is followed by the CFD results. CFD results are also consistently higher than experimental results. Another point to the capability of the model is that the offset in pressure from experimental results is fairly constant in each case. The offset is not a percentage of the measured value. The offset is between 101 and 154 Pa for each case. Likely, this is due to a component not modeled accurately enough. This could include the function used to represent the VRL. However, the relatively constant offset indicates that the physics were accurately represented. It also indicates that the model is satisfactory for comparison of different designs. Thus, the model was moved on to simulating evaporation and gasoline.

Figure 21 shows two comparisons of CFD images and experimental photos, denoted by a. and b. These were taken at comparable times prior to the respective pressure spikes at click-off. The timestamps do not match as the CFD model took slightly longer to fill. When extracting the internal volume for CFD, some internal tank components were missed, resulting in a somewhat

larger volume in the simulation. Thus, it took more time to fill the tank in simulation. However, the time between the two images is the same.

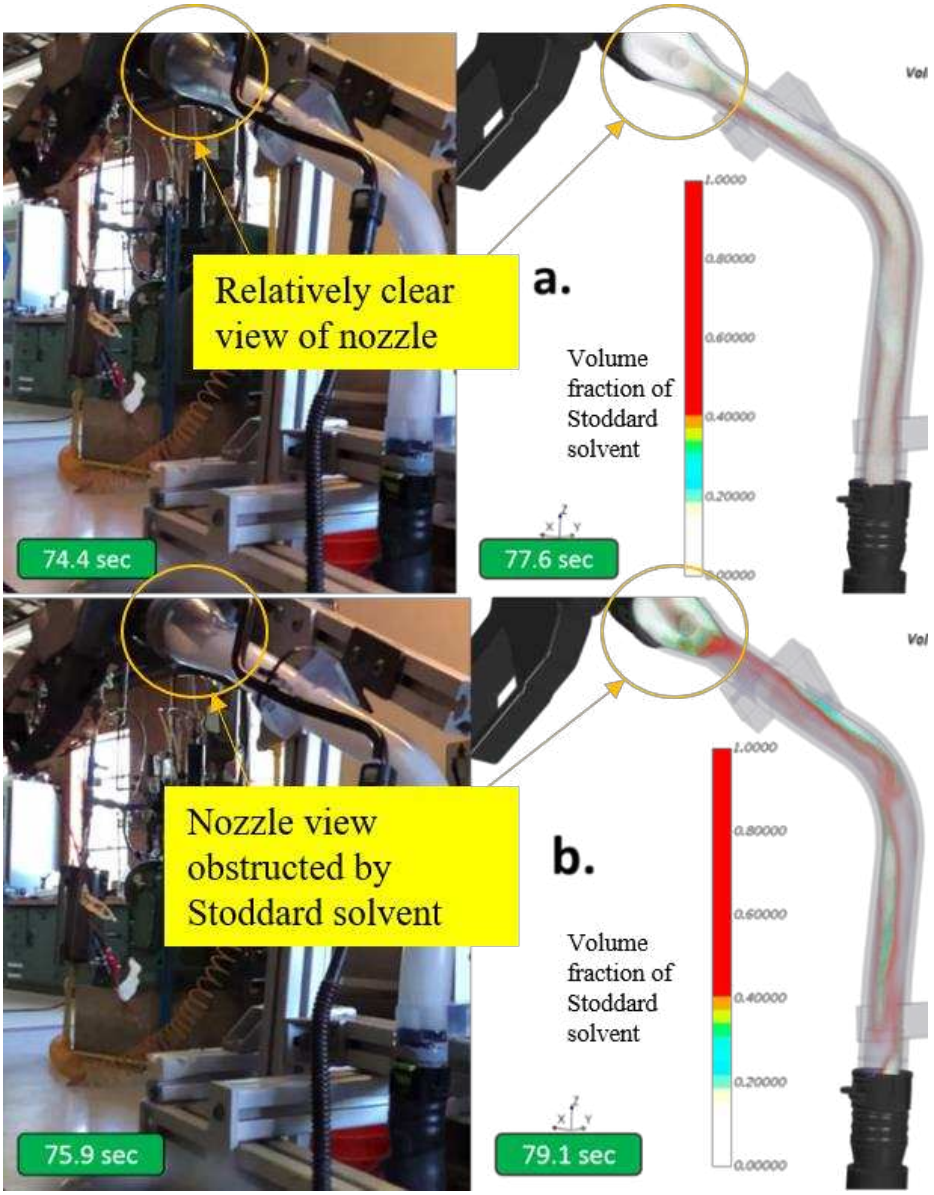

Figure 21: Visual comparison between CFD and experiment. Comparison a. shows steady state flow patterns while comparison b. shows the state just prior to click-off, 1.5 sec later.

The two comparisons visualize the flow at steady state and the moment before click-off. Of particular note is the view of the nozzle. In comparison a, there is not much fluid around the nozzle. View of the nozzle is relatively clear. However, comparison b. shows much more fluid around the nozzle and obstruction of its view. As explained in Chapter 1, liquid covering the

pressure port of the nozzle is what triggers the automatic shutoff mechanism. The qualitative comparison indicates the CFD model is predicting similar flow patterns to the physical case, including those that lead to nozzle shutoff.

4.2 Phase II – Investigation of Refueling System Emission Dynamics

Due to time and financial constraints, only one test was performed for each matrix condition. The RVP of each test is listed in Table 3. The range is from 49.43 to 55.26 kPa (7.17 to 8.01 psi). Available fuel was used and therefore does not match with the EPA regulation of 9 psi. However, as tests were conducted at elevation, with ambient pressure of approximately 12.34 psi, equilibrium headspace vapor concentrations were similar to EPA tests conducted at sea level. For fuel with 9 psi RVP at sea level and 100ºF, the equilibrium concentration would be:

$$\frac{9\ psi}{14.696\ psi} = 0.612 \qquad \text{Eq. 8}$$

For the range of RVP values measured in this study at 12.34 psi and 100ºF, the minimum and maximum concentrations would be:

$$\frac{7.17\ psi}{12.34\ psi} = 0.581 \qquad \text{Eq. 9}$$

$$\frac{8.01\ psi}{12.34\ psi} = 0.649 \qquad \text{Eq. 10}$$

Thus, the equilibrium concentrations of the current study are within 4% on either side of the EPA test concentration. Elevation and the increased equilibrium concentrations do not have a noticeable effect on refueling vapor generation, though [11]. Therefore, lower emissions and canister adsorption may be expected because of the lower RVP of the current study.

Table 3: RVP values for all cases.

RVP (kPa)	VRL 1 (1.3 Pa)	VRL 2 (255.7 Pa)	VRL 3 (827.5 Pa)
Canister 1 (123.3/141.3 Pa)	53.33	52.67	52.49
Canister 2 (219.9/239.8 Pa)	55.26	53.17	49.43
Canister 3 (331.4/357.3 Pa)	52.66	53.26	51.50

Table 4 shows the DeltaT value for each case. Each is within the set 10-13ºF range. The highest DeltaT condition occurred with the C3V2 case. The lowest occurred with the C3V3 case.

Table 4: DeltaT values for all cases.

DeltaT (ºF)	VRL 1	VRL 2	VRL 3
Canister 1	10.87	10.50	11.30
Canister 2	11.68	11.12	10.77
Canister 3	10.22	12.68	10.20

Steady state tank pressures were averaged, as in the Phase I tests. Table 5 displays the results. Note that C1V2 is the combination of original production parts. Comparison with the bar chart in Figure 18 shows a much lower tank pressure for Stoddard solvent at 10 GPM; 0.479 kPa versus 0.673 kPa with indolene at 9.8 GPM. The much greater evaporation with indolene leads to higher tank pressures.

Table 5: Average steady state tank pressures measured at the canister inlet.

SS tank P, 30-70 s into the fill (kPa)	**VRL 1**	**VRL 2**	**VRL 3**
Canister 1	0.510	0.673	0.679
Canister 2	1.204	0.841	1.276
Canister 3	1.019	1.220	2.027

The expected trend is followed for most of the cases. As the backpressure of either component increases (down or to the right in the table), the headspace pressure increases. The C2V1 case has higher than expected pressure. Note, though, that the RVP of this test is the highest, at 55.26 kPa. The next highest RVP was 53.33 kPa. The high RVP contributes to the higher than expected pressure. Mastroianni observed that RVP had a great effect on increasing tank pressure, greater effect than increasing flow rate [20]. Another point to note is the difference in pressure between the C1V2 and C1V3 cases. The increase is only 6 Pa, which is well within the noise of the pressure transducers. The reason for this negligible shift is unclear.

Table 6 shows the mass gains for each combination in the test matrix. The canister was weighed before and after each test, and the difference is the mass of HC vapors adsorbed during the test. As with the steady state pressure, the expected trend is followed in most cases. As the VRL pressure drop increases (from left to right across a row), the canister gains more vapor mass. As the canister pressure increases (from top to bottom down a column), more vapors take the VRL path and the canister adsorbs fewer HCs. The combination that interrupts this trend is C2V1. However, this higher mass gain may be explained by the high RVP of the fuel in that case.

Table 6: Canister mass gains for each case.

Canister Mass Gains (g)	**VRL 1**	**VRL 2**	**VRL 3**
Canister 1	51.0	52.5	56.3
Canister 2	55.6	47.0	51.2
Canister 3	43.5	44.3	47.2

The canister mass gains were compared with test data provided by Honda R&D Americas, Inc. The data comes from different refueling system designs, but represents typical canister mass gains for Honda refueling systems. The values obtained in the current study were lower than the data provided, but still of the same order of magnitude. The average value from the current test matrix is 31% off the average of the Honda data. The lower value is expected as the RVP of the fuel in these experiments is lower than the fuel used by Honda R&D in testing; 8.01 psi maximum in these tests versus 9 psi in Honda testing. In addition, the higher canister backpressure cases yield lower canister adsorption, lowering the average mass gain of the current study.

For the HC concentration measured at the sampling point, the opposite trend to canister vapor adsorption is expected. As VRL pressure increases, less vapor will go through the VRL. As canister pressure increases, more vapors will be sent through the VRL. The hypothesis is that less vapors through the VRL will result in less vapors escaping past the nozzle and being detected by the FID. However, as Table 7 shows, this trend is not strictly followed. The values were calculated by using the trapezoidal rule to integrate the area under the FID concentration curves. The areas were summed from nozzle insertion to one minute after shutoff. The concentration at nozzle insertion was taken as the baseline for each test. It should be noted that concentrations from the C3V1 and C3V2 cases exceeded the calibrated limit of 5000 ppm. The

exact concentration values from those cases cannot be trusted. However, the concentration traces are distinct enough to allow comparison. The IR videos also confirm the difference in emissions between those two cases and relative to the rest of the matrix.

Table 7: Emissions areas from the total test time. Baseline for integration is concentration at nozzle insertion.

Total Emissions (ppm*s)	**VRL 1**	**VRL 2**	**VRL 3**
Canister 1	35,831	43,670	25,625
Canister 2	53,882	27,947	21,271
Canister 3	4,506,437	1,690,414	27,920

Figure 22 shows HC concentration and pressure traces for the three combinations of different VRLs with Canister 1. Much variability is seen in the emissions from the time of nozzle insertion to flow start. In addition, these emissions are not accounted for in the EPA test procedure. Thus, integration from flow start to one minute after click-off was performed. The baseline was the average of the flow start and final concentrations. Table 8 shows the results. Observe that the hypothesis still does not hold for each case.

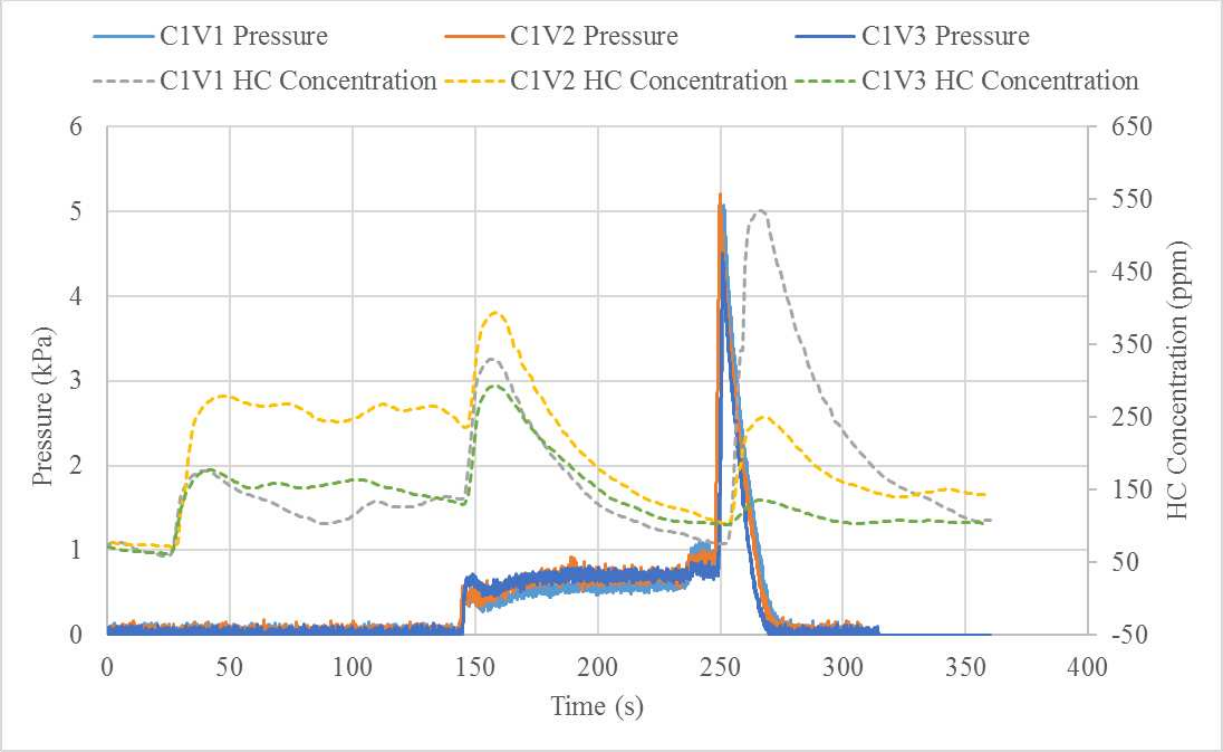

Figure 22: Plot of pressure and HC concentration for the base canister row of tests.

Table 8: Emissions areas from flow start to end of test. Baseline for integration was average of flow start and end concentrations.

Trigger to End Emissions (ppm*s)	**VRL 1**	**VRL 2**	**VRL 3**
Canister 1	11,321	2,208	5,656
Canister 2	6,442	14,825	7,360
Canister 3	4,279,184	1,524,506	1,314

Some possible reasons for the departure from the expected trend are explained in the following paragraphs. Overall, more tests are needed to improve confidence in the data. This will account for variability and allow confirmation of true physical trends.

Vapors traveling through the VRL exit into the filler pipe just downstream of the nozzle. Here some vapors are entrained in the liquid fuel flow. This effect helps to reduce ambient air

entrainment. The effects of the different components and ambient conditions on vapor and ambient air entrainment are not known. Thus, the vapor entrainment may contribute to the departure from the hypothesis.

The sampling location may also contribute uncertainty. There is a little space between the capless module and the probe where natural dilution with ambient air may occur. The dilution was not controlled or known. The air flow in the room greatly affects the dilution and may have changed from test to test or during the duration of a single test. Thus, variations in concentration may come from varying dilution and not varying emissions from the filler pipe. The FID concentrations may not be exactly proportional with or representative of total HC emissions. Further testing should be done with sampling that controls dilution. Such testing is discussed in the future works section of Chapter 5.

Looking at the pressure and concentration traces reveals more insight into the emissions dynamics. Figure 22 showed the comparison of the three cases in the Canister 1 row. The VRL pressure seems to have great effect on the final peak of the concentration trace. As the VRL pressure increases, the peak amplitude and area of the final peak of the concentration curve is reduced.

Table 9 further shows this trend. The emissions areas of the final peak most closely match the expected trend. As the VRL pressure increases, the area of the last emissions peak diminishes. It can also be seen that last peak emissions increase with increasing canister pressure. This is true in all cases except for C3V3. In fact, this case has the lowest final peak emissions, contrary to expectation.

Table 9: Last peak emissions area, defined as the area under the peak following the flow start peak and extending to one minute after click-off.

Last Peak Emissions (ppm*s)	**VRL 1**	**VRL 2**	**VRL 3**
Canister 1	12,272	4,003	791
Canister 2	13,207	10,898	1,876
Canister 3	4,214,603	1,532,430	396

Figure 23 contains the traces for the cases in the VRL 2 column. Here we can see an effect of the canister backpressure. As it increases, the start of the final peak gets pushed earlier. In the C1V2 case (the production setup), the peak starts about the same time as the pressure spike, when click-off occurs. However, as the canister pressure increases, the emissions start earlier, during the fill. In the case of Canister 3, there is only a short break between emissions from flow start to emissions exiting the filler pipe for the remainder of the fill. Table 10 shows the length of time from the beginning of the last peak to end of test for all cases. Note that if the last peak were to start at click-off, the time would be approximately 60 seconds, the length of time data was collected after click-off.

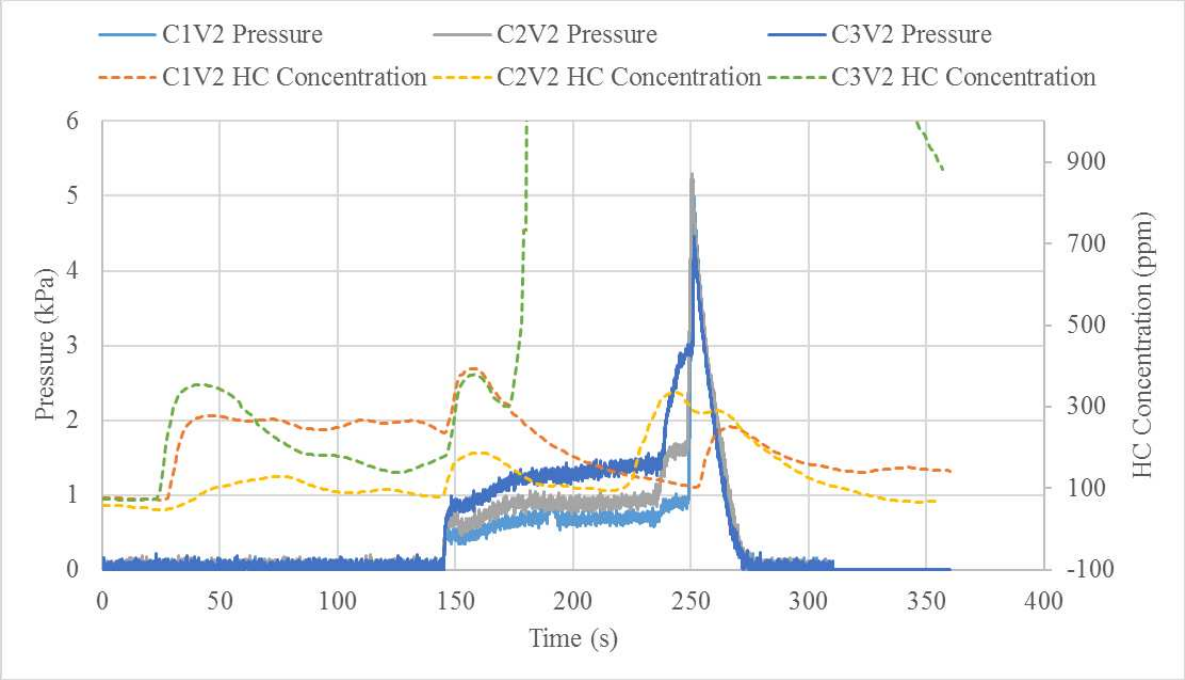

Figure 23: Plot of pressure and HC concentration for the VRL 2 column of tests.

Table 10: Length of the final emissions peak.

Last Peak Time (s)	**VRL 1**	**VRL 2**	**VRL 3**
Canister 1	63	60	60
Canister 2	62	94	61
Canister 3	145	141	75

The IR videos support these findings. Figure 24 shows two frames from the IR video of the C3V1 case, the case with the longest final peak. Vapors are seen in the image taken from approximately 20 seconds after flow is started or 85 seconds before click-off. Vapors continued to exit the filler pipe until the end of the fill.

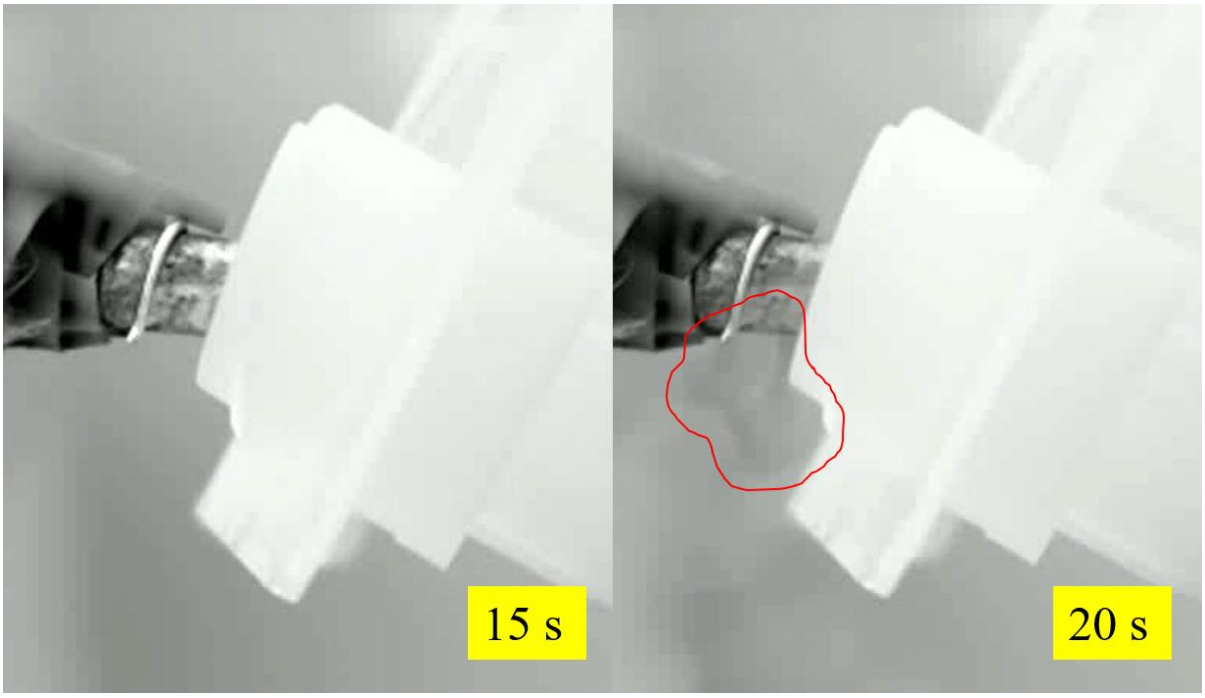

Figure 24: Emissions from the C3V1 fill. Timestamps indicate time after flow start. Note the vapors, outlined and in darker color, falling from the filler pipe at 20 seconds.

The results of the emissions exploration also indicate the timing of emissions. Figure 25 shows the concentration and pressure traces from the C1V2 case. Note again that this is the production setup. The graph shows three emissions spiking events. These coincide with nozzle insertion, flow start, and click-off. The IR images agree with these timings. Figures 26 and 27 show IR images from flow start and shutoff, respectively. The vapors in the IR video at nozzle insertion are too faint to notice in a still image.

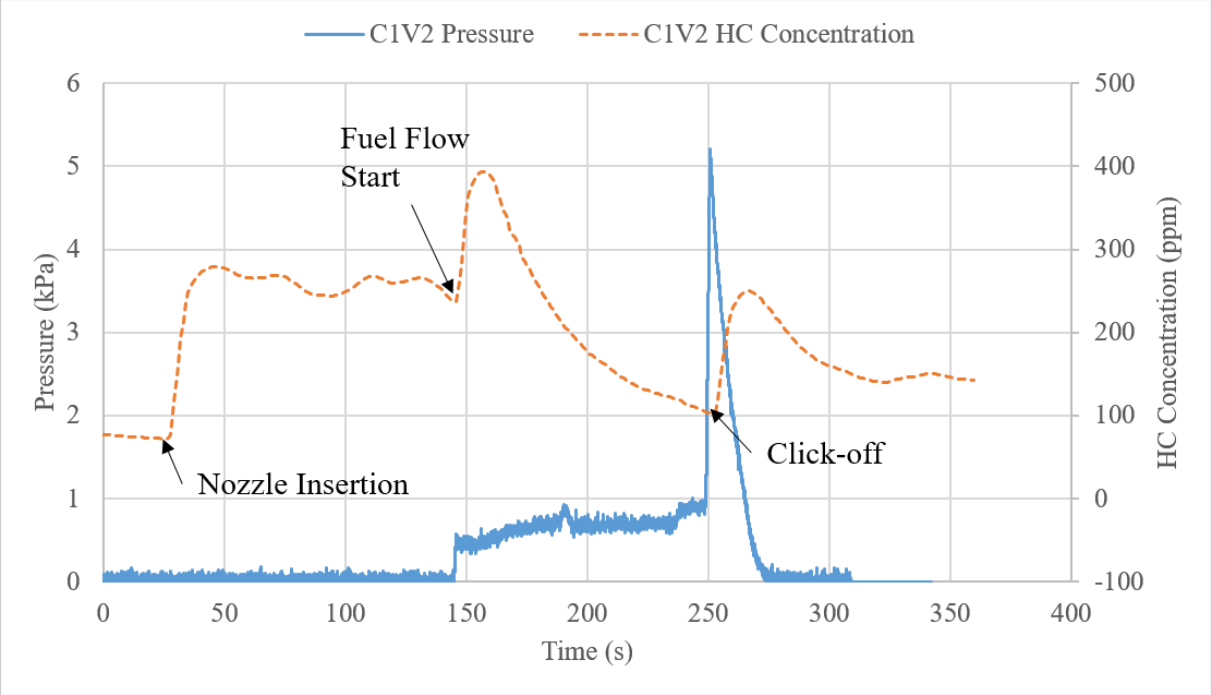

Figure 25: Plot of pressure and concentration traces for the C1V2 case. Note the three emissions spikes.

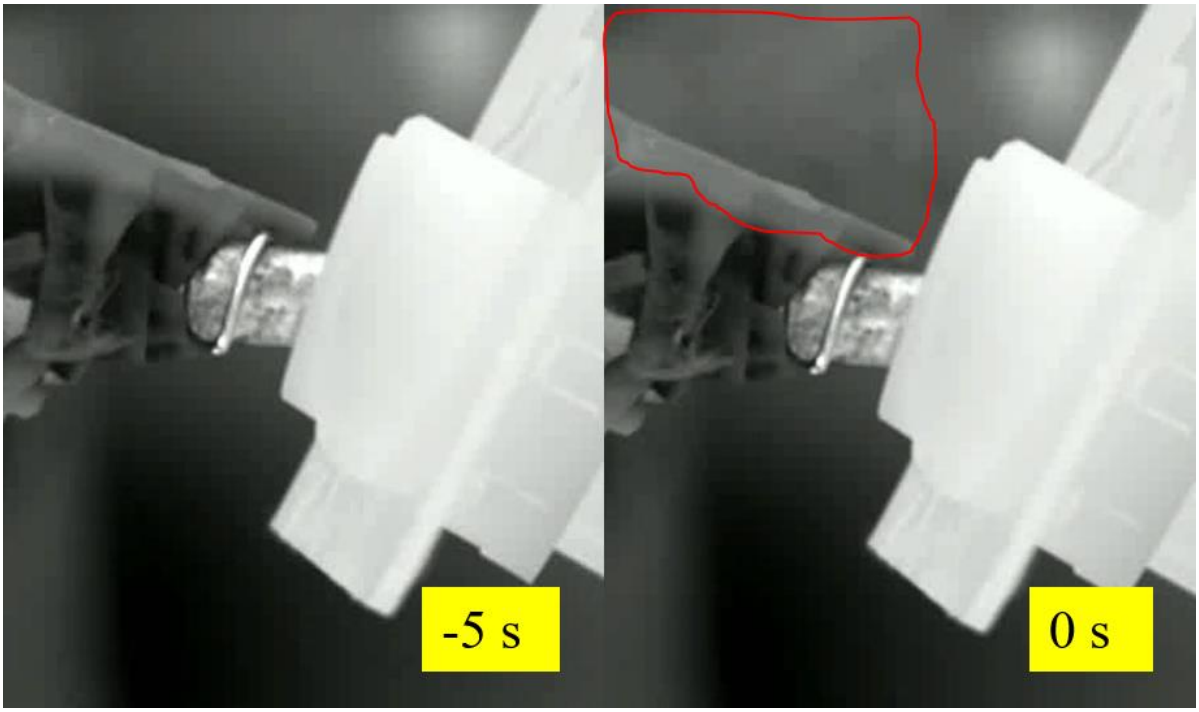

Figure 26: IR image sequence of vapor puff from flow start for the C1V2 case. Timestamps indicate time after flow start. Note the vapors at the top left of the right image, outlined and in lighter color.

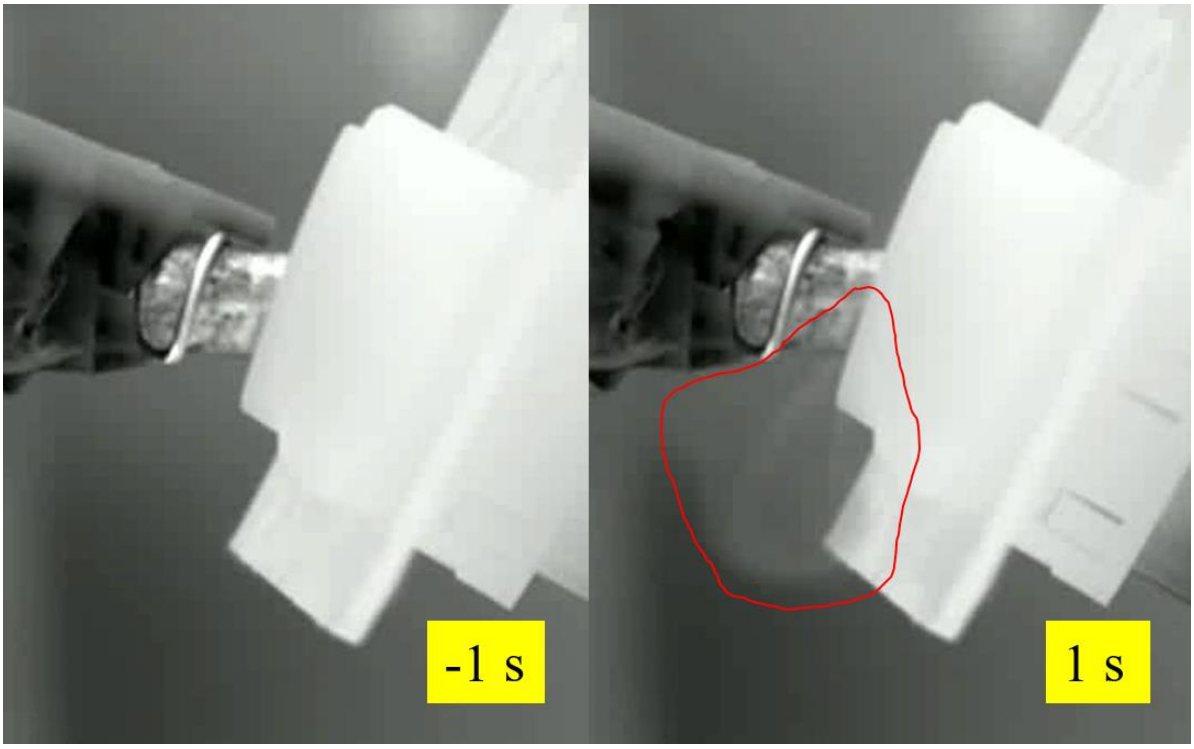

Figure 27: IR image sequence of vapor puff just after shutoff for the C1V2 case. Timestamps indicate time after click-off. Note the vapors falling from the filler pipe in the right image, outlined and in lighter color.

With knowledge of critical events, simulations can be performed in less time by simulating only those events. To verify this assumption, emissions areas were added from the 10 seconds following the start of fuel flow and final peaks. Table 11 shows the results. The expected trend (decreasing emissions with increasing VRL backpressure and increasing emissions with increasing canister backpressure) is followed by most cases. The exceptions are C2V2 and C3V3. The differences between cases in Table 11 do not match those in any of the other integrations presented in this study. Again, more tests with more control should be done to confirm the results. However, the results in Table 11 show that differences between cases can be found within the 20 seconds specified.

Table 11: Emissions areas added from 10 seconds after start of fuel flow and final peaks. Baseline for integration is the starting concentration of the respective peak.

Emissions areas from 10 s After Start of Flow and 10 s After Start of Last Peak (ppm*s)	**VRL 1**	**VRL 2**	**VRL 3**
Canister 1	2,524	1,638	952
Canister 2	3,146	861	1,132
Canister 3	46,174	4,468	350

Figure 28 shows results from a preliminary set of simulations using the critical events assumption. Only the 10 seconds after flow start and click-off were simulated. Also shown are values for the canister mass gain. From preliminary tests, contributions of the 20 seconds considered to total emissions and canister mass gain were determined. These contributions were used to obtain total values from simulation data. Both the experiments and simulations shown were performed at Honda R&D Americas, Inc. Values have been normalized. Though not able to predict the absolute value, the simulations show the same trend as the experiments between the two canisters of the respective tanks. More tests will refine assumptions and lead to more accurate predictions.

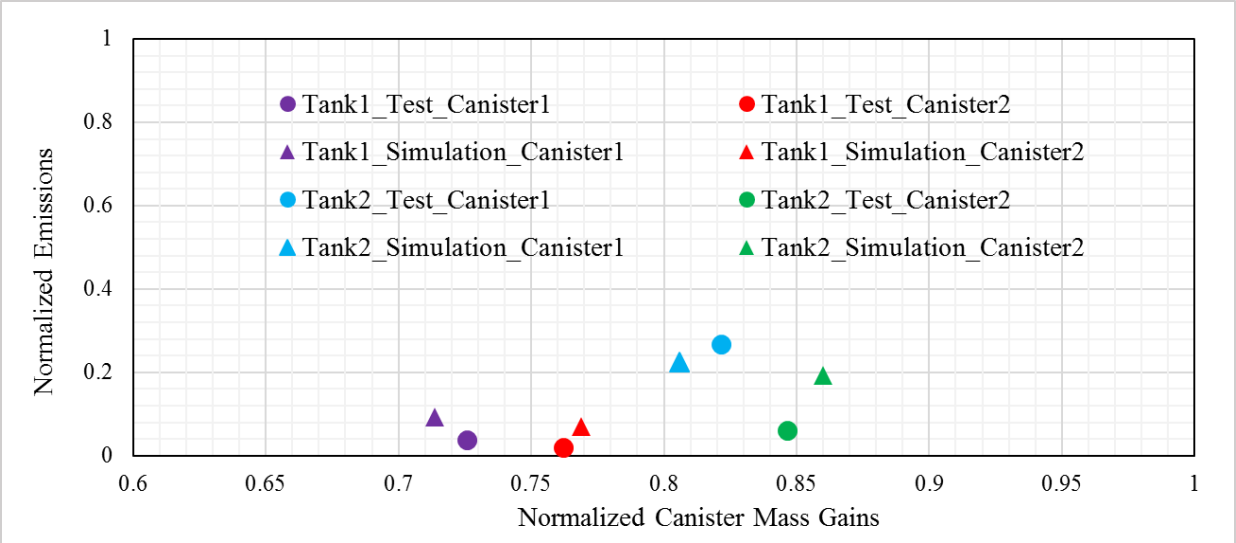

Figure 28: Normalized emissions and canister mass gain results from preliminary simulations using the critical events assumption and corresponding tests.

5. Conclusions and Future Work

5.1 Phase I – Support for CFD Model without Evaporation/Condensation

Phase I of the study was focused on providing data needed to model the full refueling system. The complex boundaries of the VRL and canister orifice were characterized. The canister orifice data validated model predictions. The VRL data was used to remove this component in simulations. Instead, a function was created from the data to predict correct flow rates through a simple outlet and inlet. Full tank filling experiments were performed with a low volatility fuel, Stoddard solvent. These were used to validate full system, non-evaporative CFD simulations. Below are some key outcomes from this part of the study:

1. The VRL and canister line were characterized by simple flow bench experiments. This allowed accurate modeling of these boundaries in CFD.
2. The test facility was created, with the refueling system configuration matching in vehicle configuration. Additionally, sensors were installed and LabVIEW programmed for data acquisition. The fuel cart and diaphragm pump were setup for fuel delivery and return, respectively. The test facility served not only for Phase I but also for continued experiments in Phase II.
3. Repeatable experiments at 4, 10, and 14 GPM were performed. Data for tank pressure, taken next to the canister inlet, was recorded. Transient fuel flow data was used to ensure experiments were performed correctly and that the fuel cart was not introducing flow disruptions.
4. Steady state, phase II of the typical refueling process, tank pressures from CFD and experiments were analyzed. Both methods show increasing tank pressure with increasing fuel

flow rate. CFD pressure values are higher than experiments by 100-150 Pa. The offset is not a function or percentage of measured values, indicating physics to be modeled correctly. Additionally, the accuracy of the model is satisfactory for comparison of designs.

5.2 Phase II – Investigation of Refueling System Emission Dynamics

Phase II of this study was focused on understanding the emissions dynamics of the refueling system. Filling tests were performed similar to the EPA refueling emissions test. Nine different combinations of VRL and canister backpressures were investigated. The effects of these backpressure on emission timing and amount has been discussed. Key findings from Phase II are listed below:

1. Timing of refueling emissions was discovered. Generally three emission events occur in connection with three refueling events. These are nozzle insertion, start of fuel flow, and nozzle click-off. Various combinations of vapor path, VRL and canister line, backpressures depart from this generalization.
2. Simulations of only critical portions of the refueling process showed the same emission and canister mass gain trends as experiments. Exact values did not match as well and will be refined in future work.
3. The effects of various combinations of vapor path backpressures on vapor travel in the refueling system were observed. Canister vapor loading increases with increasing VRL pressure and decreasing canister pressure. The effect of vapor path pressures on emissions are less clear.

5.3 Future Work

As noted previously, Phase II of the current work included only one test per case. Further understanding of changes in vapor path backpressure could be obtained with repeated

experiments. Reduced testing time would help repeat experiments. To reduce the time of tests, a better heating source could be applied to the tank; for example, an electric blanket. A better heat source would reduce the time to reach desired DeltaT.

The sampling method should be improved. Changing airflow in the laboratory affects the dilution of samples taken with the current method. In future experiments, these effects should be minimized. A possible solution would be an enclosure or shield around the nozzle and capless module. The enclosure should not be sealed as this would create a vacuum and trap emissions. The trapped emissions would interfere with the sampling by increasing the background HC concentration. Retaining the ability to measure transient emissions is crucial as SHEDs do not have this capability.

More control of temperatures and RVP would also prove helpful. These variables were accounted for as best as possible in the current study; however, true control of these parameters would provide greater confidence in the data. Variables to control would include the tank and ambient temperatures. The EPA test requires tank, pre-fill, and SHED to be at 80^{o}F. Application of a heater to increase pre-fill temperature in the current study meant tank wall temperature was greater than pre-fill temperature. Nor was the entire tank at a uniform temperature. Additionally, the ambient temperatures were not controlled; a temperature-controlled laboratory would eliminate this variable. To account for fuel weathering, RVP may be maintained by bubbling butane through the fuel. This would increase the RVP and counteract RVP decrease from evaporation of more volatile species.

The current study has observed the split of vapors between the two vapor paths in the refueling system. Critical emissions events were also found. Further tests with varying parameters, such as flow rate, should be performed to increase understanding of the emissions

dynamics. As the EPA tests may be performed at flow rates as low as 4 GPM, experiments should be conducted at this flow rate. More refueling system designs could also be incorporated. With more data from these varied conditions, especially with total HC emissions measurements in a SHED, correlations for the contribution of each emission event could be found. Such understanding would allow for the development of simplified and accurate emissions prediction tools.

References

[1] W. P. Carter, "Development of ozone reactivity scales for volatile organic compounds," *Air & waste,* vol. 44, no. 7, pp. 881-899, 1994.

[2] R. Atkinson, "Gas-phase tropospheric chemistry of organic compounds: a review," *Atmospheric Environment. Part A. General Topics,* vol. 24, no. 1, pp. 1-41, 1990.

[3] (Oct. 2018). *Code of Federal Regulations Title 40 Part 86*. Available: https://gov.ecfr.io/cgi-bin/retrieveECFR?gp=&SID=e3f2a8055e6690d4ecfc1ae8dbbbd730&mc=true&n=pt40.21.86&r=PART&ty=HTML#_top

[4] E. Lynge *et al.*, "Risk of cancer and exposure to gasoline vapors," *American journal of epidemiology,* vol. 145, no. 5, pp. 449-458, 1997.

[5] T. Tunsaringkarn, W. Siriwong, A. Rungsiyothin, and S. Nopparatbundit, "Occupational exposure of gasoline station workers to BTEX compounds in Bangkok, Thailand," *The International Journal of Occupational and Environmental Medicine,* vol. 3, no. 3, 2012.

[6] P. P. Egeghy, R. Tornero-Velez, and S. M. Rappaport, "Environmental and biological monitoring of benzene during self-service automobile refueling," *Environmental Health Perspectives,* vol. 108, no. 12, pp. 1195-1202, 2000.

[7] C. P. Weisel, "Benzene exposure: an overview of monitoring methods and their findings," *Chemico-biological interactions,* vol. 184, no. 1-2, pp. 58-66, 2010.

[8] T. Tiberi, L. Howard, and M. Heffernan. (2012, Jan. 2019). *Stage II & ORVR and Associated Emissions of Gasoline Vapor*. Available: http://www.ct.gov/deep/lib/deep/air/stageii/comments_on_draft_general_permit/arid_technologies_additional_comments_on_stage_ll_and_orvr.pdf

[9] F. Fung and B. Maxwell. (2011, Jan. 2019). *Onboard Refueling Vapor Recovery: Evaluation of the ORVR Program in the United States*. Available: https://www.theicct.org/sites/default/files/publications/ORVR_v4.pdf

[10] (2012, July 2019). *Fact Sheet: Final Rule Determining Widespread use of Onboard Refueling Vapor Recovery and Waiver of Stage Two Requirements*. Available: https://www.epa.gov/ground-level-ozone-pollution/fact-sheet-final-rule-determining-widespread-use-onboard-refueling

[11] "Evaporative and Refueling Emission Control," in *SAE Professional Development Seminars*, Detroit, 2018: SAE International.

[12] S. R. Reddy, "Mathematical models for predicting vehicle refueling vapor generation," SAE Technical Paper 2010-01-1279. doi: 10.4271/2010-01-1279

[13] R. Banerjee, K. Isaac, L. Oliver, and W. Breig, "A numerical study of automotive gas tank filler pipe two phase flow," SAE Technical Paper 2001-01-0732. doi: 10.4271/2001-01-0732

[14] R. Banerjee *et al.*, "CFD simulations of critical components in fuel filling systems," SAE Technical Paper 2002-01-0573. doi: 10.4271/2002-01-0573

[15] S. aus der Wiesche, "Simulation von Strömungen in Befüllrohren automobiler Kraftstofftanks," *Forschung im Ingenieurwesen,* vol. 68, no. 3, pp. 139-149, 2004.

[16] M. Gunnesby, "On Flow Predictions in Fuel Filler Pipe Design-Physical Testing vs Computational Fluid Dynamics," Master Thesis, Department of Management and Engineering, Linköping University, 2015.

[17] M. R. Dake, J. FitzWilliam, M. Henderson, J. Shaw, M. Swanson, and B. Windom, "Considerations for CFD Simulations of a Refueling Pump Nozzle with Application to the Computer Aided Engineering of a Vehicle Refueling System," SAE Technical Paper 2018-01-0489. doi: 10.4271/2018-01-0489

[18] P. Cingle and D. McClement, "Study of uncontrolled automotive refueling emissions," CRC-APRAC Project VE-6, 1988.

[19] H. Yamada, S. Inomata, and H. Tanimoto, "Refueling emissions from cars in Japan: Compositions, temperature dependence and effect of vapor liquefied collection system," *Atmospheric Environment,* vol. 120, pp. 455-462, 2015.

[20] M. Mastroianni, "Experimental investigation of automotive fuel tank filling," Master Thesis, Department of Mechanical, Automotive, and Materials Engineering, University of Windsor, 2000.

[21] M. C. Lockhart, "Predicting tank vapor mass for on-board refueling vapor recovery," SAE Technical Paper 970308. doi: 10.4271/970308

[22] G. A. Lavoie, Y. A. Imai, and P. J. Johnson, "A fuel vapor model (FVSMOD) for evaporative emissions system design and analysis," SAE Technical Paper 982644. doi: 10.4271/982644

[23] S. Fackrell, M. Mastroianni, and G. Rankin, "Model of the filling of an automotive fuel tank," *Mathematical and computer modelling,* vol. 38, no. 5-6, pp. 519-532, 2003.

[24] N. Sinha, R. Thompson, and M. Harrigan, "Computational simulation of fuel shut-off during refueling," SAE Technical Paper 981377. doi: 10.4271/981377

[25] "STAR-CCM+," Version 12 ed. Plano, TX: Siemens PLM, 2017.

[26] A. Hassanvand, S. Hashemabadi, and M. Bayat, "Evaluation of gasoline evaporation during the tank splash loading by CFD techniques," *International Communications in Heat and Mass Transfer,* vol. 37, no. 7, pp. 907-913, 2010.

[27] "LabVIEW," Version 15.0.1f1 ed. Austin, TX: National Instruments, 2015.

[28] T. M. Stoker, M. Dake, L. Nibbelink, M. Henderson, J. Shaw, and B. Windom, "Development and Validation of a CFD Simulation to Model Transient Flow Behavior in Automotive Refueling Systems," SAE Technical Paper 2019-01-0819. doi: 10.4271/2019-01-0819